

1 **Enabling a process-oriented hydro-biogeochemical model to simulate soil**
2 **erosion and nutrient losses**

3 Siqi Li ^{1, 2, 3}, Bo Zhu ⁴, Xunhua Zheng ^{1, 5}, Pengcheng Hu ⁴, Shenghui Han ¹, Jihui Fan ⁴, Tao
4 Wang ⁴, Rui Wang ¹, Kai Wang ¹, Zhisheng Yao ¹, Chunyan Liu ¹, Wei Zhang ^{1, *}, Yong Li ^{1, *}

5 ^{a1} State Key Laboratory of Atmospheric Boundary Layer Physics and Atmospheric Chemistry,
6 Institute of Atmospheric Physics, Chinese Academy of Sciences, Beijing 100029, China

7 ² [Institute of Carbon Neutrality, Qilu Zhongke, Jinan 250100, China](#)

8 ³ State Environmental Protection Key Laboratory of Formation and Prevention of Urban Air
9 Pollution Complex, Shanghai Academy of Environment Sciences, Shanghai 200233, China

10 ^{e4} Institute of Mountain Hazards and Environment, Chinese Academy of Sciences, Chengdu
11 610041, China

12 ^{D5} College of Earth and Planetary Science, University of Chinese Academy of Sciences, Beijing
13 100049, China

14 * Corresponding author

15 Tel.: +86 10 13681042146

16 +86 10 13107488562

17 E-mail address: zhangwei87@mail.iap.ac.cn (W. Zhang)

18 yli@mail.iap.ac.cn (Y. Li)

19

20 Abstract

21 Water-induced erosion and ~~subsequent~~associated particulate carbon (C), nitrogen (N) and
22 phosphorus (P) nutrient losses were the vital parts of biogeochemical cycling. Identifying
23 their intensity and distribution characteristics is of great significance for the control of soil
24 and water loss and N/P nonpoint source pollution. This study incorporated the modules of
25 physical soil erosion and the particulate C, N and P losses into the process-oriented
26 hydro-biogeochemical model (Catchment Nutrients Management Model coupled
27 Denitrification-Decomposition, CNMM-DNDC) to enable it to predict soil and water loss.
28 The results indicated that the upgraded CNMM-DNDC i) performed well in simulating the
29 observed temporal dynamics and magnitudes of surface runoff, sediment and particulate N/P
30 losses in the lysimetric plot of the Jieliu catchment in Sichuan Province; ii) successfully
31 predicted the observed monthly dynamics and magnitudes of stream flow, sediment yield and
32 particulate N losses at the catchment outlet, with significant ~~zero-intercept~~ univariate linear
33 regressions and ~~credible~~acceptable Nash–Sutcliffe indices ~~larger~~higher than 0.74. The
34 upgraded CNMM-DNDC demonstrated that more proportion of the particulate N to total N
35 ~~accounted for 16.2%–26.6% of the TN components~~ during the period with larger
36 precipitations than that during the droughty period (16.2%–26.6% versus 2.3%–12.4%). The
37 intensities of soil erosion and particulate nutrient losses in the Jieliu catchment was closely
38 related to land use type in the order of sloping cultivated cropland > residential area > forest
39 land. The scenario analysis demonstrated that high greenhouse gas (GHG) emissions
40 scenarios provided a greater risk of soil erosion than did low GHG emissions scenarios and

41 land use change ([i.e., from the sloping upland to forest land](#)) could help to mitigate soil and
42 water loss accelerated by climate change in the future. The upgraded model was
43 demonstrated to have the capability of predicting ecosystem productivity, hydrologic
44 nitrogen loads, emissions of GHGs and pollutant gases, soil erosion and particulate nutrient
45 losses, which [renders it a potential](#) ~~may become a~~ decision support tool for soil erosion and
46 nonpoint source pollution control coordinated with increasing production and reducing
47 GHGs and pollutant gases emissions in a catchment.

48 **Keywords**

49 CNMM-DNDC, ROSE, soil erosion, particulate carbon/nitrogen/phosphorus loss

50 **1. Introduction**

51 Water-induced erosion and ~~subsequent~~[associated](#) particulate carbon (C), nitrogen (N) and
52 phosphorus (P) nutrient losses are among the primary threats leading to the decline in soil
53 fertility and the increases in land degradation, channel sedimentation and eutrophication of
54 downstream rivers and lakes (Berhe et al., 2018; Ekholm and Lehtoranta, 2012; Garcia-Ruiz et
55 al., 2015). This global environmental issue [are becoming serious](#) ~~has continued to deteriorate~~
56 (Ma et al., 2021; Yang et al., 2003). A previous study found that the vulnerability of
57 water-induced erosion increased over 51% of the global surface from 1982 to 2015 (Liu et al.,
58 2019). Climate change and anthropogenic activities (such as land use change) are the two
59 principal driving forces that have complicated and altered the hydrological cycle and
60 water-induced erosion during recent decades (Piao et al., 2007; Zeng et al., 2015).

61 Quantitative assessments of the water-induced soil erosion intensity and identification of
62 its temporal and spatial distribution characteristics are of great importance for preventing soil

63 and water loss and have attracted the attention of researchers (e.g., Jetten et al., 2003; Jiang et
64 al., 2017; Panagos et al., 2015c). Lysimetric plot experiments have been developed as a direct
65 field measurement method for the accurate quantification of surface runoff and water-induced
66 erosion (e.g., Kosmas et al., 1997; Sumner et al., 1996; Zhu et al., 2009). However, the in situ
67 field measurements of [water-induced](#)~~water-reduced~~ soil erosion with high cost of labor and
68 money can only cover a small piece of the sampling units. It is unrealistic to expect direct field
69 measurements to quantify water-induced erosion everywhere under various conditions.

70 Simulations of mathematical models are likely to compensate for the deficiency of direct
71 field measurements [on soil erosion](#). The Universal Soil Loss Equation (USLE, Wischmeier and
72 Smith, 1978)~~and~~, its revised version (RUSLE) (Renard et al., 1997) [and its modified version](#)
73 [\(MUSLE\) \(Williams 1975\)](#) have been developed into widely used empirical mathematical
74 models to directly calculate soil erosion based on rainfall, soil property, topography, cover and
75 management data. The USLE or RUSLE quantify only the various influencing factors that
76 impact the soil loss associated with soil erosion, which is not directly related to the process of
77 surface runoff and does not involve the specific process of sediment transport yet (Donovan,
78 2022; Meinen and Robinson, 2021). Fortunately, the physical process-based ROSE model
79 named after the name of developer (Rose et al., 1983) conceptualizes the soil erosion process
80 by conceiving three continuous and simultaneous physical processes, including rainfall
81 detachment, sediment entrainment and sediment deposition, thus providing good performance
82 in estimating sediment yield at the plot scale. However, the ROSE model focuses only on the
83 physical processes of water-induced erosion without engaging the C and N cycles of the

84 ecosystem. The Soil and Water Assessment Tool (SWAT) (Arnold et al., 1998), a semi
85 distributed hydrological model, incorporates the ~~R~~USLE or MUSLE to predict soil erosion at
86 the level of hydrological response units, in which the routing of sediment transportation is not
87 considered and the modeling of the biogeochemical element cycle is relatively simple and
88 empirical (Ferrant et al., 2011; Pohlert et al., 2007). However, the transport of particulate C, N,
89 and P nutrients accompanied by water-induced erosion crucially depends on the C and N cycles
90 of ecosystems in a catchment. Previous research demonstrated that the C, N, and P contents in
91 the eroded soil were richer than that in the surface soil, which usually applied the elemental
92 enrichment module to predict (Sharply, 1980). Therefore, knowledge of the coupling between
93 the process-oriented hydro-biogeochemical model combined with the ~~complex~~~~complicated~~ C
94 and N cycles and the soil erosion model based on physical processes (~~e.g., such as~~ ROSE) is
95 essential to accurately predict soil erosion and ~~subsequent~~~~associated~~ particulate C, N, and P
96 nutrient transport.

97 A recently developed hydro-biogeochemical model (CNMM-DNDC) by Zhang et al.
98 (2018) might become a realistic tool that can be used to address the abovementioned problem.
99 The CNMM-DNDC model introduces the ~~complex~~~~complicated~~ C and N biogeochemical
100 modules (including the modules of decomposition, nitrification, denitrification and
101 fermentation) of a widely used biogeochemical model (DeNitrification-DeComposition model,
102 DNDC, Li et al., 1992) into the distributed hydrological framework of the Catchment Nutrients
103 Management Model (CNMM, Li et al., 2017). The adsorption–desorption, immobilization,
104 transposition of P element of the CNMM-DNDC model were originated from CNMM. The

105 CNMM-DNDC model has been used to conduct a comprehensive simulation of the
106 ~~complex~~~~complicated~~ hydrological and biogeochemical processes (such as ecosystem
107 productivity, hydrologic N loads, gaseous N losses and greenhouse gas emissions) of a
108 subtropical catchment with various landscapes (Zhang et al., 2018), a model evaluation of
109 nitrous oxide (N₂O) and nitric oxide (NO) emissions from a subtropical tea plantation (Zhang
110 et al., 2020b), a model evaluation and regional simulation of nitrate leaching in the black soil
111 region of Northeast China (Zhang et al., 2021a) and a comprehensive model modification and
112 evaluation of NH₃ volatilization from fertilized croplands (Li et al., 2022b). However, the
113 CNMM-DNDC model still lacks the capacity to simulate the processes of soil erosion and
114 ~~subsequent~~~~associated~~ particulate C, N, and P nutrient transportation.

115 Therefore, we hypothesize that the accurate simulation of soil erosion and
116 ~~subsequent~~~~associated~~ particulate C, N, and P nutrient losses can be realized by incorporating
117 the soil erosion physical model and the element enrichment module into the process-oriented
118 hydro-biogeochemical model with ~~complex~~~~complicated~~ C and N cycles. Based upon the above
119 hypothesis, the objectives of this study were to i) introduce the ROSE model (a physical soil
120 erosion model) and the enrichment module of the particulate nutrients into the hydrological
121 process of the CNMM-DNDC model; ii) evaluate the performance of the CNMM-DNDC
122 model in simulating the temporal and spatial distributions of soil erosion and
123 ~~subsequent~~~~associated~~ particulate C, N, and P transportation at the plot and catchment scales;
124 and iii) investigate the impact of climate change and human activities (such as land use change)
125 on the losses of soil and particulate nutrients.

2. Materials and methods

2.1 Catchment description

The Jieliu catchment (31°16'N, 105°28'E, 400–600 m a.s.l.), located in Sichuan Province of Southwest China (Zhu et al., 2009), was used for the model calibration and validation. This catchment is situated in the upper reaches of the Yangtze River and has a typical subtropical monsoon climate. During the period from 2005 to 2018, the annual mean temperature was 16.7 °C, and the average annual precipitation was 720 mm, 75% of which occurred during the period between June and September (<http://yga.cern.ac.cn>). The soil in the catchment is dominated by Calcaric purple soil, classified as a Pup-Orthic Entisol in the Chinese Soil Taxonomy or as an Entisol classified in the U.S. Soil Taxonomy (Zhu et al., 2009). The total area of the Jieliu catchment is approximately 35 ha, and it is dominated by sloping croplands (584%), [forest lands \(31%\)](#) and [the village residential areas \(10%\)](#) ~~forest lands (31%)~~. The primary crops cultivated in the sloping croplands are maize (*Zea mays* L.), winter wheat (*Triticum aestivum* L.), rape (*Brassica napus* L.) and rice (*Oryza sativa* L.). The N, P and potassium (K) fertilizers are applied at rates of 130–330 kg N ha⁻¹ yr⁻¹ (ammonium bicarbonate or urea), 72–162 kg P ha⁻¹ yr⁻¹ (calcium superphosphate) and 45–68 kg K ha⁻¹ yr⁻¹ (potassium chloride), respectively (Zhang et al., 2018). [Four replicate lysimetric plots \(an area of 8 m by 4 m with a slope gradient of 7%, Fig. 1\) were set to measure the surface runoff and the losses of the particulate N and P \(Zhu et al., 2009\). To avoid unexpected seepage, each lysimetric plot was hydrologically isolated with the cement-filled partition walls, which was inserted at least 60 cm deep into the bedrock. A conflux trough with a bucket was built at the topsoil to collect the surface runoff flow \(Zhu et al., 2009\).](#)

148 2.2 Overview of the CNMM-DNDC model

149 The CNMM-DNDC is a process-oriented hydro-biogeochemical model, which was
150 established following the basic physics, chemistry and biogeochemistry theories, through
151 incorporating the processes of C and N cycling of the DNDC into the hydrological framework
152 of the CNMM (Zhang et al., 2018). The core processes simulated by CNMM-DNDC include
153 thermal conduction, energy balance, hydraulic dynamics (e.g., soil evaporation, transpiration,
154 canopy interception, infiltration, percolation, surface runoff, subsurface flow and water uptake
155 by plants), C and N cycling (e.g., mineralization, immobilization, decomposition, nitrification,
156 denitrification, nitrate leaching, urea hydrolysis, plant uptake, and gas emissions), plant growth
157 (e.g., photosynthesis and respiration) and the discharge and water quality of the river-networks
158 (Fig. S1).

159 **2.3.2 Model modifications**

160 The CNMM-DNDC model can simulate the lateral movements of water-soluble nutrients
161 (e.g., ammonium, nitrate, phosphate and dissolved organic matter) by surface and subsurface
162 runoff, whereas it lacks the capabilities of simulating soil erosion and sediment transport
163 caused by surface runoff and the ~~subsequent~~associated transportation of particulate C, N, and P.
164 To address such a deficiency, this study incorporated the modules of soil erosion and element
165 enrichment into the lateral hydrological framework of the CNMM-DNDC model (Text S1).
166 Therefore, the upgraded CNMM-DNDC model was equipped with the ability to estimate the
167 movements of soil particles and particulate nutrients transported with surface runoff in the
168 lateral dimension (Fig. S1). The soil erosion module adopted the simplified ROSE model (Rose
169 et al., 1983; Stewart, 1985), which is a process-oriented soil erosion model. The ROSE model

170 is based on the dynamic equilibrium of three simultaneous processes, including rainfall
171 detachment, runoff detachment, and sediment deposition. In an individual erosion event, the
172 process of runoff detachment dominates, and the latter two processes of rainfall detachment
173 and sediment deposition can be generally neglected ([Stewart, 1985](#)). Therefore, in the
174 simplified ROSE module, ~~as shown by Eq. (1)~~, the sediment yield (Y_s , kg dry soil ha⁻¹)
175 resulting from soil erosion was driven by [the actual](#) surface runoff (R_s , m) and concomitantly
176 regulated by [the coverage fraction of vegetation \(\$C_v\$, fraction\) and the land's slope angle, which](#)
177 [was represented by the absolute value of the sine value of the —land's slope angle \(\$S_l\$,](#)
178 [dimensionless\)](#), ~~as shown by Eq. (1) and the coverage fraction of vegetation (C_v , fraction)~~. [The](#)
179 [complete physical processes for soil erosion of the ROSE module \(Text S2\) was the reason](#)
180 [why we chose it though the two processes which had minor effects on soil erosion in an](#)
181 [individual erosion event were neglected in the simplified ROSE module. The upgraded](#)
182 [CNMM-DNDC was expected to provide the effects of the field managements \(e.g., tillage\) on](#)
183 [soil chemical or physical properties to influence soil erosion instead of applying the empirical](#)
184 [mathematical formula to predict the effects of the field managements like what the USLE and](#)
185 [its revised or modified versions did \(Panagos et al., 2015b; Meinen and Robinson, 2021\).](#)

$$Y_s = 27 \times 10^6 (1 - C_v) \eta S_l R_s \quad (1)$$

186 Where R_s is calculated from the existing hydrological module of the CNMM-DNDC
187 model, in which R_s occurs in the following two cases. First, R_s is caused by the mechanism of
188 excess infiltration, in which the water input (i.e., precipitation and irrigation) is greater than the

189 maximum infiltration capacity of the soil. Second, R_s is derived from the mechanism of excess
190 storage, in which precipitation or irrigation still occurs when the soil surface water content
191 exceeds the corresponding saturated water content. The direction of the surface runoff conflux
192 is estimated by the distributed weights of four neighboring grids (i.e., in the upper, lower, left
193 and right directions), which are calculated based on the elevation of these grids. ~~S_i is the sine~~
194 ~~value of the slope radian value.~~ η (dimensionless) is referred to as the efficiency of sediment
195 entrained by surface runoff, which depends on soil texture and C_v , as shown in Eq. (2).

196 ~~Usually, the values of C_v need to be calibrated by the soil exposure ratio and sediment~~
197 ~~yield observations for a given study area. In this study, the value of C_v for the crop is~~
198 ~~approximately equivalent to the growing index, which is estimated by the ratio of the~~
199 ~~accumulated temperature from sowing to the present time to the accumulated thermal degree~~
200 ~~for maturity in the plant growth module. Particularly, using the observed sediment yield in the~~
201 ~~catchment outlet, the value of C_v for the natural vegetation (e.g., forest and grass) was~~
202 ~~addressed and calibrated as half of the ratio of the real leaf area index (LAI) and the maximum~~
203 ~~LAI, which is one of the model inputs. The value of C_v of the artificial lands (e.g., the urban or~~
204 ~~rural residential areas) was calibrated and set to 0.1, which represented the effects of concrete~~
205 ~~roads and residential buildings on the reduction of the soil area exposed to erosion. Usually, the~~
206 ~~values of C_v need to be calibrated by the soil exposure ratio and sediment yield observations~~
207 ~~for a given study area.~~ η (dimensionless) is referred to as the efficiency of sediment entrained
208 by surface runoff, which depends on soil texture and C_v , as shown in Eq. (2). In Eq. (2), a_1 is
209 referred to as the rate of sediment carried by surface runoff on bare land, which differs for

210 ~~various soil types and generally needs to be calibrated by the observed data of sediment loss for~~
211 ~~a given study area. Loch and Donnollan (1983) reported that a_1 varies from 1.0% to 8.7% in~~
212 ~~Middle Ridge clay loam and Irving clay soils. The soil mass balance was not considered in the~~
213 ~~upgraded model.~~

$$\eta = a_1 e^{-0.15C_v} \quad (2)$$

214 In Eq. (2), a_1 is referred to as the rate of sediment carried by surface runoff on bare land,
215 which differs for various soil textures and generally needs to be calibrated by the observed data
216 of sediment loss for a given study area. Loch and Donnollan (1983) reported that a_1 varies
217 from 1.0% to 8.7% in Middle Ridge clay loam and Irving clay soils. Among the only eight soil
218 erosion observations conducted in the lysimetric plot from 2015 to 2017, four observations in
219 2016 were provided for model calibration. More soil erosion observation of the lysimetric plots
220 with different soil textures were needed to operate the CNMM-DNDC to establish the general
221 relationship between the a_1 and soil texture (e.g., soil clay, silt and sand contents) in future.
222 Moreover, the value of C_v for the natural vegetation (e.g., forest and grass) was addressed as
223 half of the ratio of the real leaf area index (LAI) and the maximum LAI (which is one of the
224 model inputs). For the crop system, the LAI was the function of the growing index, which is
225 estimated by the ratio of the accumulated temperature from sowing to the present time to the
226 accumulated thermal degree for maturity in the plant growth module. So the C_v value of the
227 crop was calculated by the growing index. The C_v value of the artificial lands (e.g., the urban or
228 rural residential areas) was calibrated and set to 0.1, which represented the effects of concrete

229 [roads and residential buildings on the reduction of the soil area exposed to erosion. The \$C_v\$](#)
230 [value of the artificial lands might be generally quantified using the coverage of building and](#)
231 [cement roads according to more observations in future.](#)

232 It is known that the C, N, and P elements of the eroded sediments are usually richer than
233 those of the in situ soils from which the eroded sediments originate (Massey and Jackson, 1952;
234 Schiettecatte et al., 2008; Wan and El-Swaify, 1998). The above phenomenon is usually
235 referred to as sediment enrichment, which can be quantified by an empirically based
236 enrichment ratio (E). E is usually defined as the ratio of the concentration of C, N, and P
237 elements in the eroded sediment to that in the source soil (Sharpley, 1980; Teixeira and Misra,
238 2005). Generally, as more eroded sediment is produced, the richness of the C, N, and P
239 elements decreases. The enrichment ratio of the C and N nutrients (E_{CN}) is estimated by Eq. (3),
240 which was adapted from McElroy et al. (1976) and Williams and Hann (1978). The
241 pre-exponential factor (k_1) of Eq. (3) was calibrated to 1.2 using the particulate N data
242 observed at the lysimetric plot in this study. The enrichment ratio of P nutrients (E_P) is
243 calculated by Eq. (4) cited from Sharpley (1980).

$$E_{CN} = k_1(Y_s \times 10^{-4})^{-0.2468} \quad (3)$$

$$E_P = e^{(2.46 - 0.2 \log Y_s)} \quad (4)$$

244 The yields of particulate C (P_C , kg C ha⁻¹), N (P_N , kg N ha⁻¹), and P (P_P , kg P ha⁻¹)
245 nutrients caused by soil erosion were calculated based on E , Y_s and the content of the
246 corresponding organic C (C_C , g C ha⁻¹), N (C_N , g N ha⁻¹), and P (C_P , g P ha⁻¹) pools in topsoil

247 using Eqs. (5–7), respectively. BD (g m^{-3}) and D_s (m) refer to the soil bulk density and the
248 depth of topsoil, respectively. Eight of the soil organic C and N subpools participated in the
249 process of soil erosion, including the pools of very ~~reliable~~labile, ~~reliable~~labile, and resistant
250 decomposable litters, ~~reliable~~labile and resistant active microbes, ~~reliable~~labile, ~~and~~-resistant
251 ~~humads~~ and passive humus, whereas five of the soil organic P subpools were involved in the
252 process of soil erosion, including the pools of active and passive organic P, active and dead
253 microorganism P, and inert stable P. Meanwhile, the flows of C, N and P among the pools of
254 the labile and resistant organic and inorganic were considered in the CNMM-DNDC. For
255 example, the C and N of the litter and humus pools and the P of the pools of the active or
256 passive organic P and the inert stable P could flow into inorganic pools and the microbe pools
257 by decomposition. The particulate C, N, and P losses calculated by the element enrichment
258 module were also deducted from the corresponding subpools of the topsoil. Subsequently, the
259 eroded soil and the particulate C, N, and P nutrients are transported with surface runoff and
260 eventually drain into streams. The upgraded model considered the mass balances of soil water
261 and the elements of C, N, and P, without considering soil body balance.

$$P_C = \sum_{i=1}^8 \frac{10^{-7} E_{CN} C_{C_i} Y_s}{BD \cdot D_s} \quad (5)$$

$$P_N = \sum_{j=1}^8 \frac{10^{-7} E_{CN} C_{N_j} Y_s}{BD \cdot D_s} \quad (6)$$

$$P_P = \sum_{k=1}^5 \frac{10^{-7} E_P C_{P_k} Y_s}{BD \cdot D_s} \quad (7)$$

262 2.4.3 Preparation for model simulation

263 The input data for driving the model operation consisted of the meteorological data at the
264 3-hour scale (including average air temperature, solar radiation, long wave radiation, wind
265 speed, humidity and total precipitation), the spatialized soil properties (including soil texture,
266 soil organic carbon, bulk density and pH), the gridded digital elevation model (DEM, Fig. 1)
267 with a resolution of 5 m × 5 m, the spatial distribution of land use (Fig. 1) and cropping
268 systems, and the field management practices. Taking the efficiency of the model calculation
269 and the accuracy of the biogeochemical process description into consideration, the upgraded
270 CNMM-DNDC model conducted a simulation with a grid of 15 m × 15 m from 2004 to 2017,
271 with an initial spin-up period of ten years. The DEM, soil properties, land use, cropping
272 systems, field management practices and meteorological data from 2004 to 2014 were
273 primarily adapted from Zhang et al. (2018). The remaining meteorological data were adapted
274 from the hourly observations provided at the National Science & Technology Infrastructure
275 (<http://rs.cern.ac.cn>). [The information about the vertical layered soil properties \(e.g., soil bulk
276 density, pH, clay content, field capacity, wilting point, saturated hydraulic conductivity, organic
277 C, and total N and P contents\) of different land uses were listed in Table S1.](#) The input data of
278 soil properties, DEM, land use, cropping systems, and field management practices were
279 resampled to the ASCII grids with a resolution of 15 m × 15 m using the ArcGIS 10.0 software
280 package (ESRI, Redland, CA, USA). The observation data measured at the lysimetric plot and
281 the catchment outlet, [which were listed in –Table S2, \(Fig. 1\)](#) contributed to model calibration
282 and validation. The surface runoff, [subsequent associated](#) sediment yield, and particulate and

283 total N losses from 2004 to 2006 with three replicates and the surface runoff,
284 ~~subsequent~~[associated](#) sediment yield, and total P loss from 2017 to 2018 with three replicates
285 measured at the lysimetric plots were adapted from Deng et al. (2011) and Hu (2020),
286 respectively. The monthly stream flow, sediment yield, and particulate and total N losses from
287 2007 to 2008 measured at the catchment outlet were directly cited from Deng et al. (2011).
288 Total N referred to the total amount of NH_4^+ , NO_3^- , dissolved organic N and particulate N.
289 Total P referred to the total amount of dissolved organic and inorganic P and particulate P.
290 Among them, the observed data from the lysimetric plot in 2004 (with seven observation times)
291 and 2016 (with four observation times and a heavy precipitation event) and the observed data
292 from the catchment outlet in 2007 were used for model calibration, and the remaining observed
293 data were used for model validation. [Previously, a comprehensive and systematic verification](#)
294 [of the CNMM-DNDC simulation on soil temperature, soil moisture, crop yield, water flows,](#)
295 [nitrate loss, fluxes of methane, ammonia, NO and N₂O, and stream discharges of water and](#)
296 [NO₃⁻ had been conducted by Zhang et al. \(2018\), which performed statistically in good](#)
297 [agreement with the observations.](#)

298 **2.54 Climate and land use scenario settings**

299 Scenario analysis was adopted to assess the impact of climate change and land use change
300 on water-induced erosion and its accompanying nutrient losses. [The baseline scenario was set](#)
301 [as the traditional land use types and managements](#) ~~The annual accumulated yields of sediment~~
302 ~~and particulate C, N, and P nutrient losses at the outlet~~ in 2008 (the year for model validation) –
303 [with local and historical meteorology](#) ~~simulated by the upgraded model were used as the~~

304 ~~baseline values of the scenario analysis~~. Two groups of climate change and land use change
305 scenarios were designed: single-factor change and multifactor change scenarios ([Table S3](#)).
306 The single-factor change scenarios altered only one factor while keeping the others constant.
307 The single-factor change scenarios of climate change consisted of two parts. One part for air
308 temperature change was altered within the range of $-4\text{ }^{\circ}\text{C}$ to $+4\text{ }^{\circ}\text{C}$ with an interval of $0.2\text{ }^{\circ}\text{C}$ -
309 ~~(abbreviated as $T_{\text{air}+}$ the increase value of air temperature or $T_{\text{air}-}$ the decrease value of air~~
310 ~~temperature)~~. The other part for precipitation change was altered by the range from -30% to
311 $+30\%$ with an interval of 2% ~~(abbreviated as $P+$ the increase percentage of precipitation or $P-$~~
312 ~~the decrease percentage of precipitation)~~. For the sake of argument, we divided air temperature
313 and precipitation single-factor scenarios into four groups: lower and higher warming group (i.e.,
314 air temperature increased from 0°C to 2°C and from 2°C to 4°C), lower and higher cooling
315 group (i.e., air temperature decreased from 0°C to 2°C and from 2°C to 4°C); lower and higher
316 rain-enhanced group (i.e., precipitation increased from 0% to 20% and from 20% to 30%),
317 lower and higher rain-reduced group (i.e., precipitation decreased from 0% to 20% and from 20
318 to 30%). A single-factor change scenario of land use was designed as the sloping upland
319 changed into forest land with the lower soil erosion rate (i.e., UFL scenario). The existing land
320 use conversion to another type, such as the change from cropland to forest land or some other
321 land use, is a kind of compromise and required a sensitivity analysis to the model simulation
322 rather than representing the conditions of the real natural system (Dey and Mishra, 2017). ~~The~~
323 ~~multifactor change group was designed to simultaneously consider climate and land use change.~~
324 ~~The IPCC's Summary for Policy makers (IPCC, 2021) points out that the average annual~~

325 ~~global land precipitation is projected to increase by 10.5% and 30.2% at the 1.5 °C and 4 °C~~
326 ~~warming levels, respectively. According to the correspondence between climate warming and~~
327 ~~increasing precipitation in the IPCC's AR6, [The IPCC's Summary for Policy-makers \(IPCC,](#)
328 [2021\)](#) points out that the average annual global land precipitation is projected to increase by
329 [10.5% and 30.2% at the 1.5 °C and 4 °C warming levels, respectively. According to the](#)
330 [correspondence between climate warming and increasing precipitation in the IPCC's AR6,](#) the
331 multifactor change scenarios [were](#) designed [into](#) two multiple climate change scenarios: the
332 low and high greenhouse gas (GHG) emissions scenarios. The low GHG emissions scenario
333 represents air temperature and precipitation increasing by 1.5 °C and 10%, respectively, while
334 the high one represents air temperature and precipitation increasing by 4 °C and 30%,
335 respectively. ~~For the sake of argument, we also divided air temperature and precipitation~~
336 ~~single-factor scenarios into four sets. The scenarios with air temperature increases greater than~~
337 ~~2 °C were defined as the higher warming scenarios, while the lower ones were defined as the~~
338 ~~scenarios with air temperature changes from 0 °C to 2 °C. The scenarios with air temperature~~
339 ~~reductions greater than 2 °C were defined as the higher cooling scenarios, while the lower~~
340 ~~cooling scenarios were defined as the scenarios with air temperature changes from -2 °C to~~
341 ~~0 °C. Similarly, the scenarios with precipitation increases greater than 20% were defined as the~~
342 ~~higher rain-enhanced scenarios, while the lower ones were defined as the scenarios with~~
343 ~~precipitation changes from 0% to 20%. The scenarios with precipitation decreasing more than~~
344 ~~20% were defined as the higher rain-reduced scenarios, while the lower rain-reduced scenarios~~
345 ~~were defined as the scenarios with precipitation change from -20% to 0%. Furthermore, we~~~~

346 also explored the effect of the low and high GHG emissions scenarios in a combination of land
347 use change scenarios (i.e., UFL scenario) on sediment yield and particulate nutrient yields. The
348 tillage scenario analysis was involved in the scenario analysis of alternative management
349 practices, which were conducted as the no tillage operations ~~of the short term~~ in 2008 ~~and the~~
350 ~~long term from 2004 to 2008~~. The relative change deviations of the simulated annual
351 accumulated sediment and particulate nutrient losses at the catchment outlet of the designed
352 scenarios from the baseline were provided as the quantitative evaluation index for scenario
353 analysis (Abdalla et al., 2020; Dubache et al., 2019). Moreover, the crop yield changes between
354 the designed scenarios and the baseline were evaluated in the scenario analysis.

355 **2.6.5 Evaluation of model performance and statistical analysis**

356 The performance of the upgraded CNMM-DNDC model in simulating sediment and
357 particulate nutrient losses was evaluated using the normalized root mean square error (nRMSE),
358 the Nash–Sutcliffe index (NSI) and the slope, determination coefficient (R^2) and significance
359 level (p) of the ~~zero-intercept~~ univariate linear regression (~~ZIR~~ULR) between the simulation
360 and observation. The nRMSE and NSI values are calculated by Eq. 8 and Eq. 9, respectively.
361 O_i and S_i are the observed and simulated values, respectively. \bar{O} is the mean value of the
362 observed data, and n is the number of paired samples. If the value of nRMSE is closer to 100,
363 the values simulated by the model are more coincident with the observed values (Cui et al.,
364 2014; Smith et al., 1997). The value of the NSI provides the discrepancy between the simulated
365 values and the mean of the observed values, with a positive value indicating an acceptable
366 simulation (Li et al., 2022a). The closer to 1 the slope and R^2 of the ~~ZIR~~ULR are, the better the

367 simulated values match the observed values. The Origin 8.0 (OriginLab Ltd., Guangzhou,
368 China) and ArcGIS 10.0 software packages were used for graph drawing.

$$\text{nRMSE} = \frac{100}{\bar{O}} \sqrt{\frac{\sum_{i=1}^n (S_i - O_i)^2}{n}} \quad (8)$$

$$\text{NSI} = 1 - \frac{\sum_{i=1}^n (S_i - O_i)^2}{\sum_{i=1}^n (O_i - \bar{O})^2} \quad (9)$$

369 In addition, ~~linear~~ [Pearson](#) correlations were carried out to study the relationships between
370 the variables relevant to soil erosion and that related to the biogeochemistry process. [The](#)
371 [Pearson correlation coefficient \(\$r\$ \) is used to measure the correlation between two variables,](#)
372 [with the value ranging from \$-1\$ to \$1\$.](#) The R project was applied for the graph drawing of [the](#)
373 correlation matrix.

374 **3. Results**

375 **3.1 Model performance in simulating soil erosion in the lysimetric plot**

376 ~~Among the only eight soil erosion observations conducted at the lysimetric plot from 2015~~
377 ~~to 2017, four observations in 2016 were provided for model calibration.~~ Given the limited size
378 of the samples, the performance of the upgraded CNMM-DNDC model was revealed using
379 only the graph of the predictions and observations (Fig. 2a–c), without a quantitative
380 evaluation with the above statistical criteria. The temporal dynamic patterns of the simulated
381 surface runoff, sediment and concomitant particulate P yields were in accordance with the
382 observed values when either model calibration or validation was performed (Fig. 2 a–c).
383 Nevertheless, on July 23, which was a heavy precipitation event (213 mm precipitation during
384 the seven days prior to the observation day) in 2016, the upgraded model overestimated the

385 observed sediment yield by approximately 6 times (3.6 versus 0.6 t ha⁻¹, Fig. 2b). However, the
386 simulated surface runoff and total P loss were only approximately 60% and 20% larger than the
387 observed values, respectively. Unfortunately, the simulated peaks of surface runoff and
388 sediment yield at the end of June 2015 lacked the support of the observations. ~~Previous results~~
389 ~~by the authors also demonstrated that the upgraded CNMM-DNDC performed well in~~
390 ~~simulating surface runoff, sediment yield, and particulate N loss in 2004 (i.e., the verification~~
391 ~~period) in the lysimetric plot, with significant ZIRs and credible nRMSE values of 15.2%,~~
392 ~~32.0%, and 88.0%, respectively (Table S1 and Fig. 2d-g).~~ Moreover, we conducted an
393 evaluation of the simulated and observed NH₄⁺ and NO₃⁻ losses accompanied by surface runoff
394 in the lysimetric plot (Fig. S2~~†~~). The upgraded model generally captured the temporal variation
395 and magnitude of the observed NH₄⁺ and NO₃⁻ loss, although discrepancies existed in the
396 magnitude of the peak loss (i.e., the model underestimated NH₄⁺ loss caused by approximately
397 100 mm precipitation on September 4, 2006; Fig. S2~~†~~).

398 **3.2 Model performance in simulating soil erosion at the catchment outlet**

399 The monthly observed and simulated stream flow, sediment yield, particulate and total N
400 losses at the outlet of the Jieliu catchment from 2007 to 2008 are illustrated in Fig. 3. The
401 observed stream flow and sediment yield began to increase dramatically with the concentrated
402 precipitation in summer and early autumn but rarely occurred in winter and spring (Fig. 3a-c).
403 The upgraded CNMM-DNDC model successfully predicted the above temporal pattern of the
404 stream flow and sediment yield at the catchment outlet with ~~acceptable~~~~credible~~ NSI values of
405 0.89 and 0.89 and significant ~~ZIR~~~~ULR~~s with R^2 values of 0.9~~8~~~~4~~ and 0.9~~6~~~~2~~ and slope values of

406 0.9885 and 0.9088 for model validation, respectively (Table 1). Moreover, model validation of
407 sediment yield resulted in a larger nRMSE (38.23%) than that of stream flow simulation
408 (34.57%).

409 The observed particulate and total N losses revealed a similar temporal pattern to that of
410 sediment yield (Fig. 3d–e) ranged from 0 to 56.3 kg mon⁻¹ and 0.9 to 283.1 kg N mon⁻¹ with a
411 mean value of 10.5 and 55.9 kg N mon⁻¹, respectively. The corresponding simulated particulate
412 and total N losses resulted in ranges of 0.5 to 50.4 kg N mon⁻¹ and 18.8 to 196.0 kg N mon⁻¹
413 with averages of 12.0 and 65.1 kg N mon⁻¹, respectively. The upgraded model provided an
414 overestimation of the particulate N loss in August 2007 and September 2008 by 11.3 and 14.8
415 kg N mon⁻¹, respectively. The particulate N losses in February 2007, March 2007, July 2007
416 and July 2008 and total N loss in summer were underestimated. However, in terms of the
417 validation, statistical comparisons between the simulated particulate and total N losses yielded
418 significant ~~ZIR~~ULRs with R^2 values of 0.885 and 0.986 and slope values of 0.9280 and
419 1.53096, nRMSE values of 57.75% and 42.55%, and NSI values of 0.74 and 0.86, respectively
420 ($n = 12$; Table 1). Meanwhile, the upgraded CNMM-DNDC model successfully predicted the
421 temporal variation and magnitudes of NO₃⁻ loss at the catchment outlet, although the model
422 slightly underestimated the peak loss in July and August of 2007 and in September of 2008
423 (Fig. S32). The successfully prediction of the particulate N and NO₃⁻ losses and the
424 underestimation of the total N loss in July of 2007 might illustrate that the model
425 underestimated NH₄⁺ or dissolved organic N losses in July of 2007. As the above results
426 demonstrated, the simulated and observed particulate and total N losses at the catchment outlet

427 indicated good agreement despite the slight underestimation of the individual large values
428 when heavy precipitation occurred.

429 **3.3 Components of the simulated TN and PN at the catchment outlet**

430 The monthly components of TN and/or PN simulated from the original and upgraded
431 CNMM-DNDC model during the model validation of 2008 at the catchment outlet were
432 illustrated in Fig. 4. Among the TN components including PN, NH_4^+ , dissolved organic
433 ~~nitrogen~~N (DON) and NO_3^- , the simulation from both of the original and upgraded
434 CNMM-DNDC demonstrated that the proportion of NO_3^- at the catchment outlet was larger
435 than that of NH_4^+ during the period from May to September when the larger precipitations
436 appeared. Moreover, the upgraded CNMM-DNDC demonstrated that the PN accounted for up
437 to 16.2%–26.6% of the TN components during the period with larger precipitations.
438 Meanwhile, the labile or resistant humus~~humads~~ N accounted for 11.3%–20.3% of the PN
439 components, though the passive humus N accounted for the largest of the PN components. In
440 addition, compared with the original model, the upgraded model simulated the observed TN
441 with smaller nRMSE (42.55% versus 51.67%), better NSI (0.86 versus 0.80) and slightly
442 improved r^2 of the ZIRULRs (0.98 versus 0.97~~0~~) though no significant difference was found ~~of~~
443 ~~the ZIRs~~ between the original and upgraded model (Fig. 4).

444 **3.4 Spatial distributions of sediment yield and particulate C, N, and P losses**

445 Figure 5 illustrated the simulated spatial distributions of the sediment yield and particulate
446 C, N, and P losses and the effects of different land uses on those in the validation year 2008.
447 The annual accumulated sediment yield simulated by the upgraded model amounted to 0–106.6
448 $\text{t ha}^{-1} \text{ yr}^{-1}$ with an average of $5.0 \text{ t ha}^{-1} \text{ yr}^{-1}$ in 2008, which was a moderate rainfall year (952

449 mm) with eight large rainstorm events (exceeding 50 mm rainfall within 24 hours). The
450 simulated annual accumulated particulate C, N, and P losses yielded 0–595.7 kg C ha⁻¹ yr⁻¹,
451 0–56.0 kg N ha⁻¹ yr⁻¹, and 0–7.9 kg P ha⁻¹ yr⁻¹ with averages of 63.6 kg C ha⁻¹ yr⁻¹, 6.1 kg N
452 ha⁻¹ yr⁻¹ and 0.9 kg P ha⁻¹ yr⁻¹, respectively. The sloping cultivated cropland areas contributed
453 to the greatest losses of sediment and particulate C, N, and P nutrients, with 68%, 60%, 58%
454 and 57% of the total, respectively. Approximately 21% of sediment loss came from the
455 residential areas as the second largest contributor to sediment loss, while the forest areas were
456 the secondary sources to particulate C, N, and P losses, with 30%, 32%, and 32% of total losses,
457 respectively. Meanwhile, the highest rates of the particulate C, N, and P losses per unit area
458 occurred in the sloping cultivated cropland areas, with 84.1 kg C ha⁻¹ yr⁻¹, 7.7 kg N ha⁻¹ yr⁻¹
459 and 1.1 kg P ha⁻¹ yr⁻¹, respectively. However, the residential areas yielded to the highest rates
460 of sediment, i.e., 8.6 t ha⁻¹ yr⁻¹. The second largest loss rates per unit area of the particulate C,
461 N, and P appeared in the residential areas. These results demonstrated that sediment yield and
462 particulate C, N, and P losses caused by surface runoff in the Jieliu catchment were directly
463 relevant to the type of land use, and the sloping cultivated cropland area became the primary
464 source of sediment yield and particulate C, N, and P losses. Meanwhile, sediment and
465 particulate C, N, and P losses from the residential areas could not be neglected.

466 Moreover, the upgraded CNMM-DNDC model coupled the biogeochemical processes
467 with soil erosion, which was able to predict the crucial variables relevant to biogeochemical
468 processes, including the productivity, greenhouse gases, contaminated gases and NO₃⁻ loss and
469 the variables related to soil erosion, including the losses of sediment and particulate C, N and P

470 (Fig. S43, Text S1).

471 3.5 Sediment yield and particulate C, N, and P losses under different scenarios

472 The simulated results of the single-factor change scenarios of precipitation and
473 temperature were presented in Figure 6. The sediment yield and particulate C, N, and P losses
474 (i.e., the target variables) increased with precipitation or air temperature which was reflected by
475 the positive values. The more positive the slope value is, the greater the target variables
476 increase and vice versa. The slopes between the air temperature changes of the higher and
477 lower cooling and warming scenarios and the sediment yield changes yielded -1.25 , -1.00 ,
478 -0.38 and -0.40 , respectively. Compared to the slopes of the lower warming scenarios and the
479 lower cooling scenarios, the slopes of the higher warming scenarios and the higher cooling
480 scenarios provided 21% and 5% higher yields of sediment, respectively. Meanwhile, the
481 changes in particulate C, N, and P losses provided similar but stronger responses to the higher
482 cooling scenarios. However, the particulate nutrient losses showed a complicated response to
483 the warming scenarios. The changes in the particulate nutrient losses provided an increasing
484 tendency in response to the increase of air temperature. For the lower warming scenarios, the
485 particulate nutrient losses increased with air temperature. ~~The changes in the particulate~~
486 ~~nutrient losses provided an increasing tendency in response to the increase in air temperature.~~
487 In terms of the higher warming scenarios, the particulate nutrient losses were still increasing,
488 but the rates of increase rate decreased. Compared to the baseline scenario, the scenarios with
489 the air temperature change from 0 °C to -1 °C provided a slightly raising in crop yields, but the
490 crop yields were decreased as the air temperature continued to reduce. And the crop yields

491 [were reduced with the increasing air temperature.](#) These results proved that the increase in air
492 temperature decreased the losses of sediment but increased the particulate C, N, and P losses,
493 although the promoting effect became weaker for the higher warming scenarios.

494 The slopes between the precipitation changes of the higher and lower rain-reduced and
495 rain-enhanced scenarios and the sediment yield changes resulted in the values of 0.27, 0.37,
496 0.52 and 0.65, respectively. In comparison with the lower rain-enhanced and rain-reduced
497 scenarios, the slopes of the higher rain-enhanced and rain-reduced scenarios provided 24%
498 higher and 34% lower yields of sediment, respectively. Meanwhile, the changes in particulate
499 nutrient losses provided similar but weaker responses to the changes in precipitation. The
500 above results demonstrated that the losses of sediment and particulate nutrients increased with
501 the increasing precipitation. In addition, the contribution from such an elevation role of
502 precipitation tended to be stronger for the higher rain-enhanced scenarios. Furthermore, the
503 changes in sediment and particulate C, N, and P losses were more sensitive to [the](#) precipitation
504 scenarios than to [the](#) temperature scenarios. [The precipitation altered by the range from -30%
505 to +30% posed a minor influence on crop yields \(within \$\pm 0.03\%\$ \). Comparison with the
506 baseline, the scenarios with the precipitation increasing within 18% yielded to a slightly
507 increased crop yields, while crop yields slightly decreased with the scenarios of the reducing
508 precipitation and over 20% increased precipitation.](#)

509 Table 2 illustrated the results of the multifactor change scenarios and the land use change
510 single-factor scenario ([UFL](#) scenario). Compared to the baseline scenario, the [UFL](#) scenario
511 reduced stream flow, sediment yield, and particulate nutrient losses by -12.2%, -3.6%, -5.6%,

512 -7.0%, and -7.2%, respectively. In comparison with the baseline scenario, the low GHG
513 emissions scenario with air temperature increasing by 1.5 °C and precipitation increasing by
514 10% increased the stream flow, sediment yield and particulate C, N, and P losses by 21.2%,
515 4.1%, 5.3%, 5.3% and 5.3%, respectively. The increasing effects of the high GHG emissions
516 scenarios on the sediment and particulate nutrient losses were more than three times those of
517 the low GHG emissions scenarios. [The crop yield change between the low GHG emissions](#)
518 [scenario and the baseline scenario yielded to -6.0%, while the crop yield of the high GHG](#)
519 [emissions scenario accounted for 16.6% lower than the baseline.](#) The low GHG emissions
520 under the [UFL](#) scenario increased the stream flow and sediment yield by 5.2% and 0.2%,
521 respectively, but decreased the particulate C, N, and P losses by -0.8%, -2.3%, and -2.5%,
522 respectively. Moreover, the high GHG emissions under the [UFL](#) scenario increased the stream
523 flow, sediment yield, and particulate C, N, and P losses by 47.9%, 9.2%, 9.3%, 7.8%, and 7.7%,
524 respectively. The ~~short-term and long-term~~ no-tillage scenarios decreased the losses of
525 particulate nutrients by approximately ~~2.5% 1% and 20%, respectively~~, but provided [almost](#) no
526 effect on sediment yield compared with the baseline scenario ([Fig. S5](#)~~data not shown~~).

527 **3.6 Relationship among the variables relevant to soil erosion, productivity and C/N losses**

528 Figure 7 illustrated the relationships between the variables relevant to soil erosion and
529 biogeochemistry for different land use types, [which were derived from model simulation](#). No
530 soil erosion in the [winter-flooding paddy with the paddy rice-flooding fallow regime \(RF\)](#)~~RF~~
531 ~~crop-system~~ because of the year-round flooding regime. For the other three land use types, the
532 significant positive correlations ($r > 0.88$) between sediment yield and particulate nutrients

533 were found, because they were entrained by water and moved with water flow. With regard to
534 the [sloping uplands \(SU\)](#)~~SU-crop-system~~, the particulate nutrients were significantly correlated
535 with NO_3^- losses through leaching ($r > 0.6$), though the correlation coefficient between
536 sediment yields and NO_3^- losses through leaching only yielded to 0.26 (insignificantly). For the
537 [seasonally waterlogged paddy](#)~~SP-crop-system~~, the variables related to soil erosion (including
538 sediment yields and particulate nutrients) were negatively correlated with NH_3 emissions ($r >$
539 0.65), while they were positively correlated with NO_3^- losses through runoff ($r < -0.61$). As to
540 [the forest land \(FL\)](#)~~FL~~, significantly positive correlations between the variables related to soil
541 erosion and NO_3^- losses through leaching/runoff were found ($r > 0.72$), which might be
542 because all these variables were related to the precipitation. The productivity performed
543 negative impacts on sediment yield and particulate nutrients in the RF an FL systems while the
544 productivity provided a slightly negative impact on sediment yield but a slightly positive
545 impact on the particulate nutrients in the SP system.

546 **4. Discussion**

547 **4.1 Effect of land use on soil erosion and particulate C, N, and P losses**

548 Land use change has been considered one of the most important factors affecting the
549 intensity and distribution of surface runoff and soil erosion (Dunjó et al., 2004; Kosmas et al.,
550 1997; Wei et al., 2007; Zhang et al., 2021b). Our study also provided consistent results, which
551 indicated that the intensity of soil erosion and the corresponding particulate C, N, and P losses
552 in the Jieliu catchment were closely related to land use, with the following order: sloping
553 cultivated cropland > residential area > forest land. The residential area with the waterproofed
554 concrete roads and residential buildings, which was the secondary source to soil erosion, might

555 [be because it provided the largest surface runoff among these three land use types in the](#)
556 [concerned year of 2008 \(Fig. S6\), though the limited soil was exposed for erosion.](#) There were
557 three major reasons why forest land contributed to the lowest losses of sediment and particulate
558 nutrients among the above three land uses. First, canopy interception reduced the amount of
559 rainfall reaching the ground, which directly decreased the occurrence of runoff and
560 ~~subsequent~~[associated](#) erosion (Greene and Hairsine, 2004; Hou et al., 2020; Vasquez-Mendez
561 et al., 2010). Several previous studies also reported that forest land with a thick canopy
562 exhibited a lower amount of runoff than did other land uses (Mehri et al., 2018; Mohammad
563 and Adam, 2010; Nunes et al., 2011). Fortunately, the direct protection mechanism by canopy
564 interception was involved in the CNMM-DNDC model, which was calculated using the leaf
565 area index (Zhang et al., 2018). Second, the litter cover of forest land protects the soil surface
566 from the direct splash and detachment of raindrops, which can decrease the formation of
567 mechanical crusts and increase the infiltration capacity and hence diminish the potential for
568 surface runoff and soil erosion (Casermeiro et al., 2004; Lemenih et al., 2005; Wainwright et
569 al., 2002). However, the CNMM-DNDC did not take the protection of litter cover on the soil
570 surface into consideration. Further observation data and studies are needed to introduce the
571 mechanism of the effect of litter cover on surface runoff and soil sediment into the
572 CNMM-DNDC model. Last, forest land is equipped with higher soil organic matter and
573 hydraulic conductivity than other land uses, which can indirectly enhance soil infiltration and
574 reduce surface runoff (Abrishamkesh et al., 2011; Fu et al., 2000; Lemenih et al., 2004). The
575 excellent soil properties of forest land soil (e.g., higher soil organic matter and vertical

576 saturated hydraulic conductivity) have been involved in the CNMM-DNDC model inputs.
577 Moreover, as the forest litterfall returned to the soil and participated in further C and N cycling,
578 the content of soil organic matter was enhanced and accumulated. With regard to the scenario
579 analysis, we found that the scenarios related to [the forest land](#)~~FL~~ contributed to greater
580 decreases in sediment yield than surface runoff (Table 2). The results of the lysimetric plot
581 experiments by Chen et al. (2012) also demonstrated that vegetation types and human
582 interference had a relatively small impact on surface runoff but had an appreciable effect on
583 sediment yield.

584 The canopy of the cultivated cropland served as a weaker hindrance to rainfall-, [which](#)
585 [suffered from more surface runoff](#), than that of the forest canopy, ~~which suffered from more~~
586 ~~surface runoff~~. [However, the different effects on soil erosion and rainfall interception by](#)
587 [various crop planting density \(Panagos et al., 2015a\), e.g., the wide row maize and the dense](#)
588 [grass-like wheat, and different crop types \(Williamm, 1990\) needed more observations to](#)
589 [modify and evaluate the CNMM-DNDC in future](#). Furthermore, frequent agricultural activities
590 (i.e., tillage) loosen the subsurface soil and nutrients, which raises the risk of soil erosion and
591 the [associated](#)~~subsequent~~ loss of particulate nutrients (Gregorich et al., 1998; Moldenhauer et
592 al., 1967; Muukkonen et al., 2009). The CNMM-DNDC model has taken the vertical mixing
593 effect of tillage on the [chemical](#) ~~upper and lower~~ soil [properties](#) into consideration, and this
594 process left the subsurface soil organic nutrients unprotected and prone to erosion. This
595 explained the reduction in particulate C, N, and P nutrient losses under the no-tillage scenarios
596 ([Fig. S5](#)~~data not shown~~). However, several studies found that tillage disturbed the soil structure

597 and pore size distribution (Carof et al., 2007; Castellini and Ventrella, 2012; Kay and
598 VandenBygaart, 2002; Nunes et al., 2010), which made the effect of agricultural activities on
599 surface runoff and soil erosion difficult to model (Leitinger et al., 2010). Given that the vertical
600 mixing effect of tillage on soil chemical properties instead of soil physical properties was ~~not~~
601 considered in the CNMM-DNDC, the yields of surface runoff and sediment resulting from the
602 no-tillage scenario were not decreased compared with the baseline scenario with tillage (Fig.
603 S5).

604 **4.2 Effect of climate change on soil erosion and particulate C, N, and P losses**

605 In past decades, the frequent occurrence of warming and extreme weather events (e.g.,
606 extreme precipitation events) has been irrefutable (IPCC, 2019). From 1998 to 2021, the
607 observed annual average air temperature and annual precipitation in the Jieliu catchment also
608 presented an increasing trend but did not have a significant regression relationship (Fig. S4S7).
609 In CNMM-DNDC, the biogeochemical processes were strongly influenced by air or soil
610 temperature (Table S4). There were two reasons ~~of~~ why the simulated soil erosion responded to
611 the air temperature changes. On one hand, the vegetation growth was sensitive to the air
612 temperature changes, which ~~might be that the climate-sensitive vegetation growth~~ affected the
613 C_v which was the effect factor of the soil erosion in Eq. 1. The increasing air temperature
614 provided a positive effect on the vegetation growth (e.g., leaf area index, Fig. S8), which
615 increased the precipitation interception by canopy to direct decrease the soil erosion. However,
616 the raising air temperature might shorten the duration of the vegetation growth period, which
617 directly shortened the period of the soils protected by crop canopy and lengthened the time of

618 the bare soils exposed to the surface runoff increasing the risk of erosion (Fig. S8). This
619 increasing risk of sediment yield when air temperature increased was not shown in this case
620 might because that the heavy rainfall events almost occurred the duration with vegetation
621 growth (Fig. S8). Besides, the decreasing air temperature weakened the processes of the
622 respiration and photosynthesis, which led to a slower vegetation growth (Fig. S8). On the other
623 hand, compared to the baseline scenarios, the climate warming scenarios, with a better
624 vegetation growth, conducted a higher evapotranspiration, which led to a reduction on soil
625 moisture content, to indirectly reduce the surface runoff and soil erosion. The asymmetric
626 response of sediment yield and particulate nutrient losses to the cooling and warming scenarios
627 might result from the different ~~effects response~~ of the cooling and warming of air temperature
628 on the vegetation growth ~~to the cooling and warming of air temperature~~. The growth of
629 vegetation was strongly inhibited by the low temperature in the cooling scenarios through
630 affecting the duration and start time of the phenological stages. Our results of the scenario
631 analysis indicated that the losses of sediment slightly decreased with the scenarios treated with
632 climate warming alone, which lay in the higher C_v caused by the enhanced vegetation growth
633 (Ficklin et al., 2009; Zhang et al., 2020a; Zhou et al., 2003). We found that the decreasing
634 effect of increasing air temperature on sediment loss decreased (especially for the scenario with
635 an air temperature increase of 4 °C, Fig. 6), which might be because the enhanced effect of
636 increasing air temperature on vegetation growth is not unlimited. Once the air temperature
637 exceeds the threshold of the optimum temperature for photosynthesis and vegetation growth, it
638 would have a negative or even harmful impact on plant growth (Chapin, 1983; Schlenker and

639 Roberts, 2009). The complex response of the particulate C, N, and P losses to air temperature
640 increased, probably because they increased with ~~ER~~the enrichment ratio and sediment yield,
641 but the enrichment ratio~~ER~~ decreased with sediment. Therefore, the slightly increasing
642 sediment with increasing air temperature and the corresponding decreasing enrichment ratio~~ER~~
643 might lead to upward or downward fluctuations in particulate C, N, and P losses. However, we
644 found that the rate of soil loss increased with increasing precipitation amount and the
645 corresponding increase in heavy rain events. Jiang et al. (2017) also found that the increase in
646 sediment loss was amplified by the increased precipitation, which was directly accompanied by
647 a dramatic and sustained increase in surface runoff. Therefore, the higher GHG emissions
648 scenarios, in which the soil erosion provided a higher increase response to the rising
649 precipitation and a lower and smaller decrease response to the rising air temperature, might
650 provide a greater risk of soil erosion than the low GHG emissions scenario. Overall, our results
651 indicated that the hydrology of the Jieliu catchment is very sensitive to potential future climate
652 changes, especially to the higher GHG emissions scenarios.

653 **4.3 Interactive effect of climate and land use change on soil and nutrient losses**

654 Changes in either climate or land use imply considerable influences on water and nutrient
655 cycles in a catchment or region (Labat et al., 2004; Milliman et al., 2008; Piao et al., 2007; Yin
656 et al., 2017). Our simulated results indicated that the reduction extent of the UFL scenario ~~with~~
657 ~~FL~~ on soil erosion, especially on sediment yield and associated~~subsequent~~ nutrient losses,
658 offset the increasing extent caused by the low GHG emissions scenario. However, the UFL
659 scenario ~~with FL~~ was insufficient to totally offset the sediment and particulate C, N, and P

660 losses caused by the high GHG emissions scenario. Nevertheless, vegetation restoration might
661 still be able to slow the soaring process of soil erosion caused by climate change in the future.
662 Previous studies primarily focused on the effects of human activity and climate change on the
663 changes in surface runoff or stream flow. Wang et al. (2016) demonstrated that human activity
664 contributed to slightly larger effects on stream flow changes than climate (59% versus 41%) by
665 analyzing the long-term records of hydrological data in the Luan River basin in North China.
666 The results in the Heihe River basin in Northwest China showed that human activities were the
667 dominant contributor to the variation in runoff in the upper and middle reaches when compared
668 to climate change (Qiu et al., 2015). However, other studies have shown that the influence of
669 climate change on soil and water loss was greater than that of human activities. Jiang et al.
670 (2017) pointed out that climate change, in comparison with anthropogenic activities, was the
671 primary factor causing the changes in either stream flow or sediment discharge in the Yellow
672 River basin and Yangtze River basin in China. The Huron River catchment in southeastern
673 Michigan in the U.S.A. was more sensitive to climate change than to land use change, as
674 demonstrated by Barlage et al. (2002).

675 Furthermore, we found that the promoting impacts of both high and low GHG emissions
676 scenarios on surface runoff were greater than those on sediment yield and ~~associated~~~~subsequent~~
677 particulate nutrient losses. In contrast, the reduction effect of the UFL scenarios ~~with FL~~ on
678 sediment yield and ~~subsequent~~~~associated~~ particulate nutrient losses was stronger than that on
679 surface runoff (Table 2). These results demonstrated that human activity, e.g., the conversion
680 from cropland with intensive human disturbance to forest land, resulted in a greater mitigation

681 effect on sediment yield and ~~associated~~~~subsequent~~ particulate nutrient losses than on surface
682 runoff. Therefore, further studies should consider the effects of human activity and climate
683 change on surface runoff and on soil erosion as well as the ~~associated~~~~subsequent~~ nutrient losses.
684 In summary, reasonable human intervention, such as rational land use change, is expected to be
685 a feasible practice to decelerate soil erosion and ~~subsequent~~~~associated~~ particulate nutrient
686 losses without altering and disturbing the hydrological cycle of a catchment in the context of
687 global warming.

688 **Conclusions**

689 The hydro-biogeochemical model (CNMM-DNDC) was improved by introducing the soil
690 erosion physical model (adopted from the simplified ROSE model) and the element (i.e.,
691 carbon, nitrogen and phosphorus) enrichment module to estimate soil erosion and the
692 movements of particulate nutrients. The comparability between the simulation and observation,
693 including surface runoff, sediment yield, and particulate nitrogen and phosphorus losses at the
694 lysimetric plot and the stream flow, sediment yield, and particulate N loss at the outlet of Jieliu
695 catchment, demonstrated that the upgraded CNMM-DNDC model could reliably simulate soil
696 erosion and the consequential particulate nutrient losses. The spatial distribution characteristics
697 of sediment yield and the consequential particulate carbon, nitrogen and phosphorus losses
698 were directly related to the spatial distribution of land use type, among which the sloping
699 cultivated cropland areas contributed to the greatest losses. The analysis of climate
700 single-factor change scenarios implied that the high GHG emissions scenarios provided a
701 greater potential risk of soil erosion, which resulted in the larger soil erosion rates than those in

702 the low GHG emissions scenarios. The scenarios with all non-forest land changes into forest
703 land decreased stream flow, sediment yield and particulate C, N, and P losses compared to the
704 baseline scenario. Anthropogenic activities (e.g., land use change) might be expected to help
705 mitigate the processes of soil and water losses accelerated by climate change in the future.

706 **Code and data availability**

707 The CNMM-DNDC model was originally developed by the Institute of Atmospheric
708 Physics using C++ language, which can be run on a standard PC. The upgraded model is
709 available on the FigShare (<https://doi.org/10.6084/m9.figshare.20210546>).

710 **Author contribution**

711 Siqi Li arranged data, improved model and implemented the simulation, prepared the
712 original draft. Yong Li, Xunhua Zheng, Wei Zhang developed the conceptualization and
713 methodology of this study. Bo Zhu, Pengcheng Hu, Jihui Fan, Tao Wang collected and
714 arranged data. Shenghui Han, Rui Wang, Kai Wang analyzed data and verified the results.
715 Zhisheng Yao, Chunyan Liu improved the conceptualization and writing.

716 **Acknowledgments**

717 This work was supported by the Chinese Academy of Sciences (grant number:
718 ZDBS-LY-DQC007; XDA23070100), [the National Key R&D Program of China \(grant number:
719 2022YFE0209200\)](#), the special fund of State Environmental Protection Key Laboratory of
720 Formation and Prevention of Urban Air Pollution Complex ([grant number:
721 SEPAir-2022080590](#)), the National Key Scientific and Technological Infrastructure project
722 “Earth System Science Numerical Simulator Facility” (EarthLab), the National Natural Science
723 Foundation of China (grant number: 41907280, U22A20562), and the China Postdoctoral

724 Science Foundation (grant number: 2019M650808).

725 **Competing interests**

726 The authors declare that they have no conflict of interest.

727 **References**

728 Abdalla, M., Song, X., Ju, X., Topp, C., and Smith, P.: Calibration and validation of the
729 DNDC model to estimate nitrous oxide emissions and crop productivity for a summer
730 maize-winter wheat double cropping system in Hebei, China, *Environmental Pollution*, 262,
731 114199, <https://doi.org/10.1016/j.envpol.2020.114199>, 2020.

732 Abrishamkesh, S., Gorji, M., and Asadi, H.: Long-term effects of land use on soil
733 aggregate stability, *International Agrophysics*, 25, 103–108,
734 [http://www.international-agrophysics.org/Long-term-effects-of-land-use-on-soil-aggregate-stab](http://www.international-agrophysics.org/Long-term-effects-of-land-use-on-soil-aggregate-stability,106297,0,2.html)
735 [ility,106297,0,2.html](http://www.international-agrophysics.org/Long-term-effects-of-land-use-on-soil-aggregate-stability,106297,0,2.html), 2011.

736 Arnold, J., Srinivasan, R., Muttiah, R., and Williams, J.: Large area hydrologic modeling
737 and assessment part I: model development, *Journal of the American Water Resources*
738 *Association*, 34, 73–89, <https://doi.org/10.1111/j.1752-1688.1998.tb05961.x>, 1998.

739 Barlage, M., Richards, P., Sousounis, P., and Brenner, A.: Impacts of climate change and
740 land use change on runoff from a Great Lakes watershed, *Journal of Great Lakes Research*, 28,
741 568–582, [https://doi.org/10.1016/S0380-1330\(02\)70606-0](https://doi.org/10.1016/S0380-1330(02)70606-0), 2002.

742 Berhe, A., Barnes, R., Six, J., and Marin-Spiotta, E.: Role of Soil Erosion in
743 Biogeochemical Cycling of Essential Elements: Carbon, Nitrogen, and Phosphorus, *Annual*
744 *Review of Earth and Planetary Sciences*, 46, 521–548,
745 <https://doi.org/10.1146/annurev-earth-082517-010018>, 2018.

746 Carof, M., De Tourdonnet, S., Coquet, Y., Hallaire, V., and Roger-Estrade, J.: Hydraulic
747 conductivity and porosity under conventional and no-tillage and the effect of three species of
748 cover crop in northern France, *Soil Use and Management*, 23, 230–237,
749 <https://doi.org/10.1111/j.1475-2743.2007.00085.x>, 2007.

750 Casermeiro, M., Molina, J., Caravaca, M., Costa, J., Massanet, M., and Moreno, P.:
751 Influence of scrubs on runoff and sediment loss in soils of Mediterranean climate, *Catena*, 57,
752 91–107, [https://doi.org/10.1016/s0341-8162\(03\)00160-7](https://doi.org/10.1016/s0341-8162(03)00160-7), 2004.

753 Castellini, M. and Ventrella, D.: Impact of conventional and minimum tillage on soil
754 hydraulic conductivity in typical cropping system in Southern Italy, *Soil and Tillage Research*,
755 124, 47–56, <https://doi.org/10.1016/j.still.2012.04.008>, 2012.

756 Chapin, F.: Direct and indirect effects of temperature on arctic plants, *Polar Biology*, 2,
757 47–52, <https://doi.org/10.1007/BF00258285>, 1983.

758 Chen, H., Yang, J., Fu, W., He, F., and Wang, K.: Characteristics of slope runoff and
759 sediment yield on karst hill-slope with different land-use types in northwest Guangxi,
760 *Transactions of the Chinese Society of Agricultural Engineering*, 28, 121–126,
761 <https://doi.org/10.3969/j.issn.1002-6819.2012.16.019>, 2012.

762 Cui, F., Zheng, X., Liu, C., Wang, K., Zhou, Z., and Deng, J.: Assessing biogeochemical
763 effects and best management practice for a wheat-maize cropping system using the DNDC
764 model, *Biogeosciences*, 11, 91–107, <https://doi.org/10.5194/bg-11-91-2014>, 2014.

765 Deng, J., Zhou, Z., Zhu, B., Zheng, X., Li, C., Wang, X., and Jian, Z.: Modeling nitrogen
766 loading in a small watershed in southwest China using a DNDC model with hydrological

767 enhancements, *Biogeosciences*, 8, 2999–3009, <https://doi.org/10.5194/bg-8-2999-2011>, 2011.

768 Dey, P. and Mishra, A.: Separating the impacts of climate change and human activities on
769 streamflow: a review of methodologies and critical assumptions, *Journal of Hydrology*, 548,
770 278–290, <https://doi.org/10.1016/j.jhydrol.2017.03.014>, 2017.

771 Donovan, M.: Modelling soil loss from surface erosion at high-resolution to better
772 understand sources and drivers across land uses and catchments; a national-scale assessment of
773 Aotearoa, New Zealand, *Environmental Modelling & Software*, 147, 105228,
774 <https://doi.org/10.1016/j.envsoft.2021.105228>, 2022.

775 Dubache, G., Li, S., Zheng, X., Zhang, W., and Deng, J.: Modeling ammonia
776 volatilization following urea application to winter cereal fields in the United Kingdom by a
777 revised biogeochemical model, *Science of The Total Environment*, 660, 1403–1418,
778 <https://doi.org/10.1016/j.scitotenv.2018.12.407>, 2019.

779 Dunjó, G., Pardini, G., and Gispert, M.: The role of land use–land cover on runoff
780 generation and sediment yield at a microplot scale, in a small Mediterranean catchment,
781 *Journal of Arid Environments*, 57, 99–116, [https://doi.org/10.1016/S0140-1963\(03\)00097-1](https://doi.org/10.1016/S0140-1963(03)00097-1),
782 2004.

783 Ekholm, P. and Lehtoranta, J.: Does control of soil erosion inhibit aquatic eutrophication,
784 *Journal of Environmental Management*, 93, 140–146,
785 <https://doi.org/10.1016/j.jenvman.2011.09.010>, 2012.

786 Ferrant, S., Oehler, F., Durand, P., Ruiz, L., Salmon-Monviola, J., Justes, E., Dugast, P.,
787 Probst, A., Probst, J., and Sanchez-Perez, J.: Understanding nitrogen transfer dynamics in a

788 small agricultural catchment: comparison of a distributed (TNT2) and a semi distributed
789 (SWAT) modeling approaches, *Journal of Hydrology*, 406, 1–15,
790 <https://doi.org/10.1016/j.jhydrol.2011.05.026>, 2011.

791 Ficklin, D., Luo, Y., Luedeling, E., and Zhang, M.: Climate change sensitivity assessment
792 of a highly agricultural watershed using SWAT, *Journal of Hydrology*, 374, 16–29,
793 <https://doi.org/10.1016/j.jhydrol.2009.05.016>, 2009.

794 Fu, B., Chen, L., Ma, K., Zhou, H., and Wang, J.: The relationships between land use and
795 soil conditions in the hilly area of the loess plateau in northern Shaanxi, China, *Catena*, 39,
796 69–78, [https://doi.org/10.1016/s0341-8162\(99\)00084-3](https://doi.org/10.1016/s0341-8162(99)00084-3), 2000.

797 Garcia-Ruiz, J., Begueria, S., Nadal-Romero, E., Gonzalez-Hidalgo, J., Lana-Renault, N.,
798 and Sanjuan, Y.: A meta-analysis of soil erosion rates across the world, *Geomorphology*, 239,
799 160–173, <https://doi.org/10.1016/j.geomorph.2015.03.008>, 2015.

800 Greene, R. and Hairsine, P.: Elementary processes of soil-water interaction and thresholds
801 in soil surface dynamics: a review, *Earth Surface Processes and Landforms*, 29, 1077–1091,
802 <https://doi.org/10.1002/esp.1103>, 2004.

803 Gregorich, E., Greer, K., Anderson, D., and Liang, B.: Carbon distribution and losses:
804 erosion and deposition effects, *Soil and Tillage Research*, 47, 291–302,
805 [https://doi.org/10.1016/S0167-1987\(98\)00117-2](https://doi.org/10.1016/S0167-1987(98)00117-2), 1998.

806 Hou, G., Bi, H., Huo, Y., Wei, X., Zhu, Y., Wang, X., and Liao, W.: Determining the
807 optimal vegetation coverage for controlling soil erosion in *Cynodon dactylon* grassland in
808 North China, *Journal of Cleaner Production*, 244, 118771,

809 <https://doi.org/10.1016/j.jclepro.2019.118771>, 2020.

810 Hu, P.: Applicability of revised DNDC model to simulate phosphorus migration on the
811 slope farmland of purple soil, Institute of Mountain Hazards and Environment, University of
812 Chinese Academy of Sciences, Chengdu, 2020.

813 IPCC: Climate Change and Land: an IPCC Special Report on Climate Change,
814 Desertification, Land Degradation, Sustainable Land Management, Food Security, and
815 Greenhouse Gas Fluxes in Terrestrial Ecosystems, 2019.

816 IPCC: Sixth Assessment Report: Working Group I: Summary for Policemakers, 2021.

817 Jetten, V., Govers, G., and Hessel, R.: Erosion models: quality of spatial predictions,
818 *Hydrological Processes*, 17, 887–900, <https://doi.org/10.1002/hyp.1168>, 2003.

819 Jiang, C., Zhang, L., and Tang, Z.: Multi-temporal scale changes of streamflow and
820 sediment discharge in the headwaters of Yellow River and Yangtze River on the Tibetan
821 Plateau, China, *Ecological Engineering*, 102, 240–254,
822 <https://doi.org/10.1016/j.ecoleng.2017.01.029>, 2017.

823 Kay, B. and VandenBygaart, A. : Conservation tillage and depth stratification of porosity
824 and soil organic matter, *Soil and Tillage Research*, 66, 107–118,
825 [https://doi.org/10.1016/S0167-1987\(02\)00019-3](https://doi.org/10.1016/S0167-1987(02)00019-3), 2002.

826 Kosmas, C., Danalatos, N., Cammeraat, L., Chabart, M., Diamantopoulos, J., Farand, R.,
827 Gutierrez, L., Jacob, A., Marques, H., Martinez-Fernandez, J., Mizara, A., Moustakas, N.,
828 Nicolau, J., Oliveros, C., Pinna, G., Puddu, R., Puigdefabregas, J., Roxo, M., Simao, A.,
829 Stamou, G., Tomasi, N., Usai, D., and Vacca, A.: The effect of land use on runoff and soil

830 erosion rates under Mediterranean conditions, *Catena*, 29, 45–59,
831 [https://doi.org/10.1016/S0341-8162\(96\)00062-8](https://doi.org/10.1016/S0341-8162(96)00062-8), 1997.

832 Labat, D., Godderis, Y., Probst, J., and Guyot, J.: Evidence for global runoff increase
833 related to climate warming, *Advances in Water Resources*, 27, 631–642,
834 <https://doi.org/10.1016/j.advwatres.2004.02.020>, 2004.

835 Leitinger, G., Tasser, E., Newesely, C., Obojes, N., and Tappeiner, U.: Seasonal dynamics
836 of surface runoff in mountain grassland ecosystems differing in land use, *Journal of Hydrology*,
837 385, 95–104, <https://doi.org/10.1016/j.jhydrol.2010.02.006>, 2010.

838 Lemenih, M., Karlton, E., and Olsson, M.: Assessing soil chemical and physical property
839 responses to deforestation and subsequent cultivation in smallholders farming system in
840 Ethiopia, *Agriculture, Ecosystems & Environment*, 105, 373–386,
841 <https://doi.org/10.1016/j.agee.2004.01.046>, 2005.

842 Lemenih, M., Olsson, M., and Karlton, E.: Comparison of soil attributes under *Cupressus*
843 *lusitanica* and *Eucalyptus saligna* established on abandoned farmlands with continuously
844 cropped farmlands and natural forest in Ethiopia, *Forest Ecology and Management*, 195, 57–67,
845 <https://doi.org/10.1016/j.foreco.2004.02.055>, 2004.

846 Li, C., Frolking, S., and Frolking, T.: A model of nitrous oxide evolution from soil driven
847 by rainfall events: 1. Model structure and sensitivity, *Journal of Geophysical*
848 *Research–Atmospheres*, 97, 9759–9776, <https://doi.org/10.1029/92jd00509>, 1992.

849 Li, S., Li, Y., Zhang, W., Zheng, X., Hu, P., Fan, J., Wang, T., and Zhu, B.: Simulation of
850 water-induced erosion and transport of particulate elements in catchment by extending the

851 CNMM-DNDC model, Chinese Journal of Eco-Agriculture, [30\(9\), 1511–1521](#),
852 <https://doi.org/10.12357/cjea.20210781>, 2022a.

853 Li, S., Zhang, W., Zheng, X., Li, Y., Han, S., Wang, R., Wang, K., Yao, Z., Liu, C., and
854 Zhang, C.: Update a biogeochemical model with process-based algorithms to predict ammonia
855 volatilization from fertilized uplands and rice paddy fields, Biogeosciences, 2022, 3001–3019,
856 <https://doi.org/10.5194/bg-19-3001-2022>, 2022b.

857 Li, Y., Shen, J., Wang, Y., Gao, M., Liu, F., and Zhou, P.: CNMM: a grid-based
858 spatially-distributed catchment simulation model, China Science Press, Beijing, 2017.

859 Liu, Y., Fu, B., Liu, Y., Zhao, W., and Wang, S.: Vulnerability assessment of the global
860 water erosion tendency: vegetation greening can partly offset increasing rainfall stress, Land
861 Degradation & Development, 30, 1061–1069, <https://doi.org/10.1002/ldr.3293>, 2019.

862 Loch, R. and Donnollan, T.: Field rainfall simulator studies on two clay soils of the
863 Darling Downs, Queensland. II. Aggregate breakdown, sediment properties and soil erodibility,
864 Australian Journal of Soil Research, 21, 47–58, <https://doi.org/10.1071/sr9830047>, 1983.

865 Ma, X., Zhao, C., and Zhu, J.: Aggravated risk of soil erosion with global warming: a
866 global meta-analysis, Catena, 200, 105129, <https://doi.org/10.1016/j.catena.2020.105129>,
867 2021.

868 Massey, H. and Jackson, M.: Selective erosion of soil fertility constituents, Soil Science
869 Society of America Proceedings, 16, 353–356,
870 <https://doi.org/10.2136/sssaj1952.03615995001600040008x>, 1952.

871 McElroy, A., Chiu, S., Nebgen, J., and Bennett, F.: Loading functions for assessment of

872 water pollution from nonpoint sources, Midwest Research Institute, Kansas City, 1976.

873 Mehri, A., Salmanmahiny, A., Tabrizi, A., Mirkarimi, S., and Sadoddin, A.: Investigation
874 of likely effects of land use planning on reduction of soil erosion rate in river basins: case study
875 of the Gharesoo River Basin, *Catena*, 167, 116–129,
876 <https://doi.org/10.1016/j.catena.2018.04.026>, 2018.

877 Meinen, B. and Robinson, D.: From hillslopes to watersheds: Variability in model
878 outcomes with the USLE, *Environmental Modelling & Software*, 146, 105229,
879 <https://doi.org/10.1016/j.envsoft.2021.105229>, 2021.

880 Milliman, J., Farnsworth, K., Jones, P., Xu, K., and Smith, L.: Climatic and anthropogenic
881 factors affecting river discharge to the global ocean, 1951–2000, *Global and Planetary Change*,
882 62, 187–194, <https://doi.org/10.1016/j.gloplacha.2008.03.001>, 2008.

883 Mohammad, A. and Adam, M.: The impact of vegetative cover type on runoff and soil
884 erosion under different land uses, *Catena*, 81, 97–103,
885 <https://doi.org/10.1016/j.catena.2010.01.008>, 2010.

886 Moldenhauer, W., Wischmei, W., and Parker, D.: Influence of crop management on runoff
887 erosion and soil properties of a Marshall silty clay loam, *Soil Science Society of America*
888 *Proceedings*, 31, 541–546, <https://doi.org/10.2136/sssaj1967.03615995003100040031x>, 1967.

889 Muukkonen, P., Hartikainen, H., and Alakukku, L.: Effect of soil structure disturbance on
890 erosion and phosphorus losses from Finnish clay soil, *Soil and Tillage Research*, 103, 84–91,
891 <https://doi.org/10.1016/j.still.2008.09.007>, 2009.

892 Nunes, A., de Almeida, A., and Coelho, C.: Impacts of land use and cover type on runoff

893 and soil erosion in a marginal area of Portugal, *Applied Geography*, 31, 687–699,
894 <https://doi.org/10.1016/j.apgeog.2010.12.006>, 2011.

895 Nunes, A., Coelho, C., de Almeida, A., and Figueiredo, A.: Soil erosion and hydrological
896 response to land abandonment in a central inland area of Portugal, *Land Degradation &*
897 *Development*, 21, 260–273, <https://doi.org/10.1002/ldr.973>, 2010.

898 [Panagos P., Borrelli P., Meusburger K., Alewell C.: Lugato E., Montanarella L.:](#)
899 [Estimating the soil erosion cover-management factor at the European scale, *Land Use Policy*,](#)
900 [48, 38–50, <https://doi.org/10.1016/j.landusepol.2015.05.012>, 2015a.](#)

901 [Panagos P., Borrelli P., Meusburger K., Zanden E., Poesen J., Alewell C.: Modelling the](#)
902 [effect of support practices \(P-factor\) on the reduction of soil erosion by water at European](#)
903 [scale. *Environmental science & policy*, 51, 23–34,](#)
904 <http://dx.doi.org/10.1016/j.envsci.2015.03.012>, 2015b.

905 Panagos, P., Borrelli, P., and Robinson, D.: Tackling soil loss across Europe, *Nature*, 526,
906 195, <https://doi.org/10.1038/526195d>, 2015c.

907 Piao, S., Friedlingstein, P., Ciais, P., de Noblet-Ducoudré, N., Labat, D., and Zaehle, S.:
908 Changes in climate and land use have a larger direct impact than rising CO₂ on global river
909 runoff trends, *Proceedings of the National Academy of Sciences of the United States of*
910 *America*, 104, 15242–15247, <https://doi.org/10.1073/pnas.0707213104>, 2007.

911 Pohlert, T., Huisman, J., Breuer, L., and Frede, H.: Integration of a detailed
912 biogeochemical model into SWAT for improved nitrogen predictions: model development,
913 sensitivity, and GLUE analysis, *Ecological Modelling*, 203, 215–228,

914 <https://doi.org/10.1016/j.ecolmodel.2006.11.019>, 2007.

915 Qiu, L., Peng, D., Xu, Z., and Liu, W.: Identification of the impacts of climate changes
916 and human activities on runoff in the upper and middle reaches of the Heihe River basin, China,
917 *Journal of Water and Climate Change*, 7, 251–262, <https://doi.org/10.2166/wcc.2015.115>,
918 2015.

919 Renard, K., Foster, G., Weesies, G., McCool, D., and Yoder, D.: Predicting soil erosion by
920 water: a guide to conservation planning with the Revised Universal Soil Loss equation
921 (RUSLE), Agricultural Handbook Service, United States Department of Agriculture,
922 Washington, 1997.

923 Rose, C., Williams, J., Sander, G., and Barry, D.: A mathematical model of soil erosion
924 and deposition processes: I. theory for a plane land element, *Soil Science Society of America*
925 *Journal*, 47, 991–995, <https://doi.org/10.2136/sssaj1983.03615995004700050030x>, 1983.

926 Schiettecatte, W., Gabriels, D., Cornelis, W., and Hofman, G.: Enrichment of organic
927 carbon in sediment transport by interrill and rill erosion processes, *Soil Science Society of*
928 *America Journal*, 72, 50–55, <https://doi.org/10.2136/sssaj2007.0201>, 2008.

929 Schlenker, W. and Roberts, M.: Nonlinear temperature effects indicate severe damages to
930 US crop yields under climate change, *Proceedings of the National Academy of Sciences of the*
931 *United States of America*, 106, 15594–15598, <https://doi.org/10.1073/pnas.0906865106>, 2009.

932 Sharpley, A.: The enrichment of soil Phosphorus in runoff sediments, *Journal of*
933 *Environmental Quality*, 9, 521–526, <https://doi.org/10.2134/jeq1980.00472425000900030039x>,
934 1980.

935 Smith, P., Smith, J., Powlson, D., McGill, W., Arah, J., Chertov, O., Coleman, K., Franko,
936 U., Frolking, S., Jenkinson, D., Jensen, L., Kelly, R., Klein-Gunnewiek, H., Komarov, A., Li,
937 C., Molina, J., Mueller, T., Parton, W., Thornley, J., and Whitmore, A.: A comparison of the
938 performance of nine soil organic matter models using datasets from seven long-term
939 experiments, *Geoderma*, 81, 153–225, [https://doi.org/10.1016/s0016-7061\(97\)00087-6](https://doi.org/10.1016/s0016-7061(97)00087-6), 1997.

940 Stewart, B.: *Advance in soil science*, Springer-Verlag, New York Berlin Heidelberg Tokyo,
941 18–55, 1985.

942 Sumner, H., Wauchope, R., Truman, C., Dowler, C., and Hook, J.: Rainfall simulator and
943 plot design for mesoplot runoff studies, *Transactions of the ASAE*, 39, 125–130,
944 <https://doi.org/10.13031/2013.27489>, 1996.

945 Teixeira, P. and Misra, R.: Measurement and prediction of nitrogen loss by simulated
946 erosion events on cultivated forest soils of contrasting structure, *Soil and Tillage Research*, 83,
947 204–217, <https://doi.org/10.1016/j.still.2004.07.014>, 2005.

948 Vasquez-Mendez, R., Ventura-Ramos, E., Oleschko, K., Hernandez-Sandoval, L., Parrot,
949 J., and Nearing, M.: Soil erosion and runoff in different vegetation patches from semiarid
950 Central Mexico, *Catena*, 80, 162–169, <https://doi.org/10.1016/j.catena.2009.11.003>, 2010.

951 Wainwright, J., Parsons, A., Schlesinger, W., and Abrahams, A.: Hydrology–vegetation
952 interactions in areas of discontinuous flow on a semi-arid bajada, Southern New Mexico,
953 *Journal of Arid Environments*, 51, 319–338, <https://doi.org/10.1006/jare.2002.0970>, 2002.

954 Wan, Y. and El-Swaify, S.: Sediment enrichment mechanisms of organic carbon and
955 phosphorus in a well-aggregated Oxisol, *Journal of Environmental Quality*, 27, 132–138,

956 <https://doi.org/10.2134/jeq1998.00472425002700010019x>, 1998.

957 Wang, H., Chen, L., and Yu, X.: Distinguishing human and climate influences on
958 streamflow changes in Luan River basin in China, *Catena*, 136, 182–188,
959 <https://doi.org/10.1016/j.catena.2015.02.013>, 2016.

960 Wei, W., Chen, L., Fu, B., Huang, Z., Wu, D., and Gui, L.: The effect of land uses and
961 rainfall regimes on runoff and soil erosion in the semi-arid loess hilly area, China, *Journal of*
962 *Hydrology*, 335, 247–258, <https://doi.org/10.1016/j.jhydrol.2006.11.016>, 2007.

963 [Williamm J.: The erosion-productivity impact calculator \(EPIC\) model: a case history,](#)
964 [Philosophical Transactions of the Royal Society, 329, 421–428,](#)
965 <https://doi.org/10.1098/rstb.1990.0184>, 1990.

966 [Williams, J.: Sediment routing for agricultural watersheds, Journal of the American Water](#)
967 [Resources Association, 11, 965–974, https://doi.org/10.1111/j.1752-1688.1975.tb01817.x,](#)
968 [1975.](#)

969 Williams, J. and Hann, R.: Optimal operation of large agricultural watersheds with water
970 quality constraints, Texas Water Resource Institute, Texas A&M University, Texas, 1978.

971 Wischmeier, W. and Smith, D.: Predicting rainfall erosion losses: a guide to conservation
972 planning, *Agricultural Handbook*, Science and Education Administration, United States
973 Department of Agriculture, Washington, 1978.

974 Yang, D., Kanae, S., Oki, T., Koike, T., and Musiakke, K.: Global potential soil erosion
975 with reference to land use and climate changes, *Hydrological Processes*, 17, 2913–2928,
976 <https://doi.org/10.1002/hyp.1441>, 2003.

977 Yin, J., He, F., Xiong, Y., and Qiu, G.: Effects of land use/land cover and climate changes
978 on surface runoff in a semi-humid and semi-arid transition zone in northwest China, *Hydrology
979 and Earth System Sciences*, 21, 183–196, <https://doi.org/10.5194/hess-21-183-2017>, 2017.

980 Zeng, S., Zhan, C., Sun, F., Du, H., and Wang, F.: Effects of climate change and human
981 activities on surface runoff in the Luan river basin, *Advances in Meteorology*, 6, 1–12,
982 <https://doi.org/10.1155/2015/740239>, 2015.

983 Zhang, F., Shi, X., Zeng, C., Wang, L., Xiao, X., Wang, G., Chen, Y., Zhang, H., Lu, X.,
984 and Immerzeel, W.: Recent stepwise sediment flux increase with climate change in the Tuotuo
985 River in the central Tibetan Plateau, *Science Bulletin*, 65, 410–418,
986 <https://doi.org/10.1016/j.scib.2019.12.017>, 2020a.

987 Zhang, W., Li, Y., Zhu, B., Zheng, X., Liu, C., Tang, J., Su, F., Zhang, C., Ju, X., and
988 Deng, J.: A process-oriented hydro-biogeochemical model enabling simulation of gaseous
989 carbon and nitrogen emissions and hydrologic nitrogen losses from a subtropical catchment,
990 *Science of the Total Environment*, 616, 305–317,
991 <https://doi.org/10.1016/j.scitotenv.2017.09.261>, 2018.

992 Zhang, W., Yao, Z., Zheng, X., Liu, C., Wang, R., Wang, K., Li, S., Han, S., Zuo, Q., and
993 Shi, J.: Effects of fertilization and stand age on N₂O and NO emissions from tea plantations: a
994 site-scale study in a subtropical region using a modified biogeochemical model, *Atmospheric
995 Chemistry and Physics*, 20, 6903–6919, <https://doi.org/10.5194/acp-20-6903-2020>, 2020.

996 Zhang, W., Li, S., Han, S., Zheng, X., Xie, H., Lu, C., Sui, Y., Wang, R., Liu, C., Yao, Z.,
997 and Li, T.: Less intensive nitrate leaching from Phaeozems cultivated with maize generally

998 occurs in northeastern China, *Agriculture, Ecosystems & Environment*, 310, 107303,
999 <https://doi.org/10.1016/j.agee.2021.107303>, 2021a.

1000 Zhang, X., Song, J., Wang, Y., Deng, W., and Liu, Y.: Effects of land use on slope runoff
1001 and soil loss in the Loess Plateau of China: a meta-analysis, *Science of The Total Environment*,
1002 755, 142418, <https://doi.org/10.1016/j.scitotenv.2020.142418>, 2021b.

1003 Zhou, L., Kaufmann, R., Tian, Y., Myneni, R., and Tucker, C.: Relation between
1004 interannual variations in satellite measures of northern forest greenness and climate between
1005 1982 and 1999, *Journal of Geophysical Research-Atmospheres*, 108, ACL 3-1–ACL 3-16,
1006 <https://doi.org/10.1029/2002jd002510>, 2003.

1007 Zhu, B., Wang, T., Kuang, F., Luo, Z., Tang, J., and Xu, T.: Measurements of nitrate
1008 leaching from a hillslope cropland in the Central Sichuan Basin, China, *Soil Science Society of
1009 America Journal*, 73, 1419–1426, <https://doi.org/10.2136/sssaj2008.0259>, 2009.

1010

1011 Table 1 Performance of the ~~upgraded~~revised CNMM-DNDC model in simulating the stream
 1012 flow, sediment, and particulate and total nitrogen (N) losses at the Jieliu catchment outlet from
 1013 2007 to 2008. Total N refers to the total amount of NH₄⁺, NO₃⁻, dissolved organic N and
 1014 particulate N.

Variables	Operation	Size	nRMSE	NSI	ULR ZIR		
					Slope	R ²	p
Stream flow	Calibration	12	18.29	0.98	0.94 5	0.96 8	< 0.001
	Validation	12	34.57	0.89	0.98 85	0.98 4	< 0.001
Sediment loss	Calibration	12	34.02	0.94	0.96 1	0.93 6	< 0.001
	Validation	12	38.23	0.89	0.90 88	0.96 2	< 0.05
Particulate N loss	Calibration	12	49.45	0.87	0.78 93	0.85 8	< 0.001
	Validation	12	57.75	0.74	0.92 80	0.88 5	< 0.001
Total N loss	Calibration	12	56.98	0.86	1.36 21	0.98 0	< 0.001
	Validation	12	42.55	0.86	1.53 0.96	0.98 86	< 0.001

1015 The statistical criteria used to quantify the discrepancy between observations and simulations
 1016 include the normalized root mean square error (nRMSE), the Nash–Sutcliffe index (NSI) and
 1017 the slope, determination coefficient (R²) and significance level (p) of the ~~zero-intercept~~
 1018 univariate linear regression (ULR~~ZIR~~). Size represents the sample size. The column
 1019 “Operation” represents the evaluation is conducted for model calibration or validation.

1020

1021

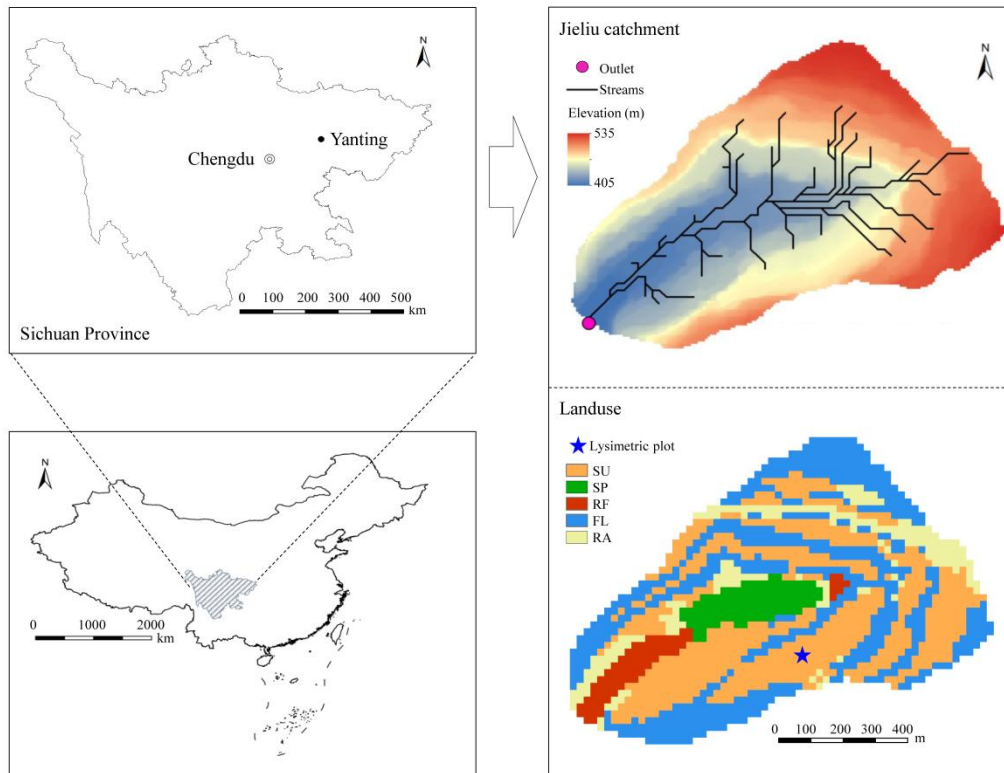
1022 Table 2 Simulated comprehensive effects of precipitation, air temperature and land use change
 1023 on [crop yield \(Yield\)](#), surface runoff, sediment yield, and particulate carbon (C), nitrogen (N)
 1024 and phosphorus (P) losses in the validation year of 2008. The low greenhouse gas (GHG)
 1025 emission scenario represents the scenario of air temperature increasing by 1.5°C and
 1026 precipitation increasing by 10%. The high GHG emission scenario represents the scenario of an
 1027 air temperature increase of 4°C and a precipitation increase of 30%. The [UFL](#) scenario is the
 1028 abbreviation of the scenario of upland change into forest land.

Scenario	Change between the scenario and the baseline (%)					
	Surface runoff	Sediment yield	Particulate C	Particulate N	Particulate P	Yield
Low GHG	21.2	4.1	5.3	5.3	5.3	-6.0
High GHG	72.9	14.8	17.8	18.0	18.1	-16.6
UFL	-12.2	-3.6	-5.6	-7.0	-7.2	-
Low GHG with UFL	5.2	0.2	-0.8	-2.3	-2.5	-
High GHG with UFL	47.9	9.2	9.3	7.8	7.7	-

1029

1030

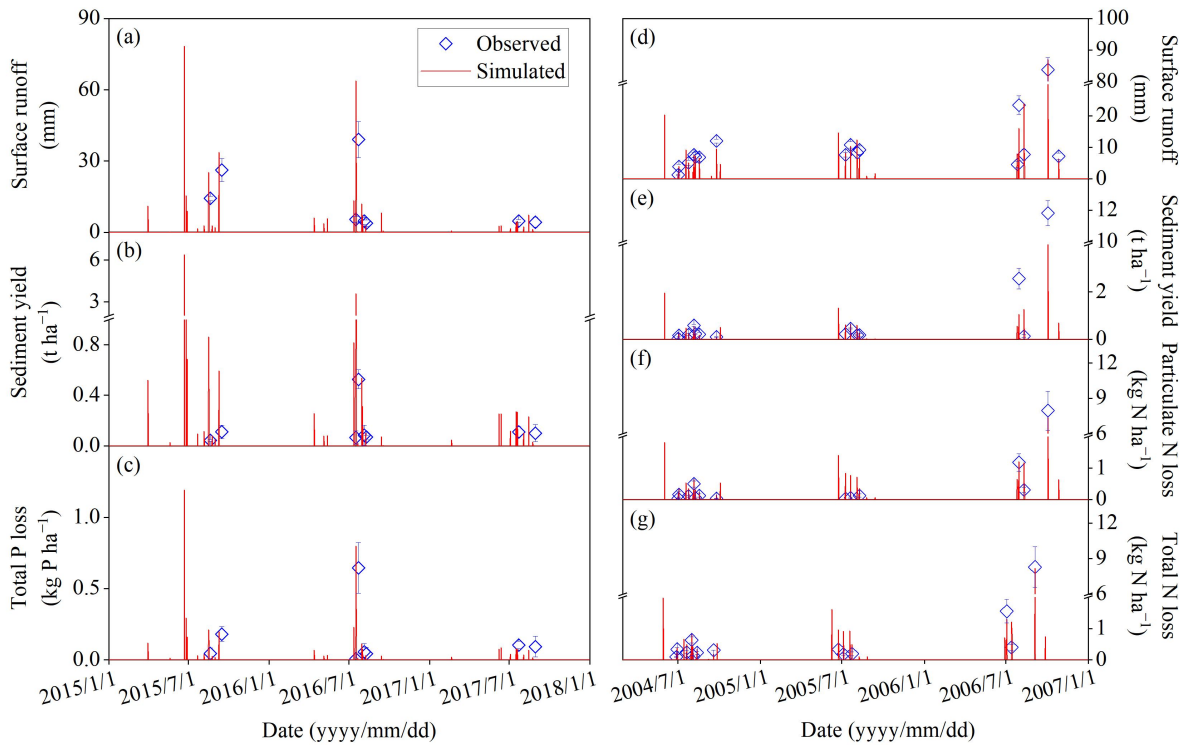
1031



1032

1033 Fig. 1 The location, digital elevation model and land use types of the Jieliu catchment. The land
1034 use types are the sloping uplands (SU) with the summer maize–winter wheat rotation (SU),
1035 seasonally waterlogged paddy (SP) with the paddy rice–winter wheat rotation or paddy
1036 rice–rape rotation (SP), the winter-flooding paddy with the paddy rice-flooding fallow regime
1037 (RF), and the forest land (FL) and the village residential area (RA).

1038



1039

1040 Fig. 2 Observed and simulated surface runoff (a), sediment yield (b) and total phosphorus (P)

1041 losses (c) from 2015 to 2017 and surface runoff (d), sediment yield (e), particulate nitrogen (N)

1042 loss (f) and total N loss (g) from 2015 to 2017 in the lysimetric plot. Total P refers to the

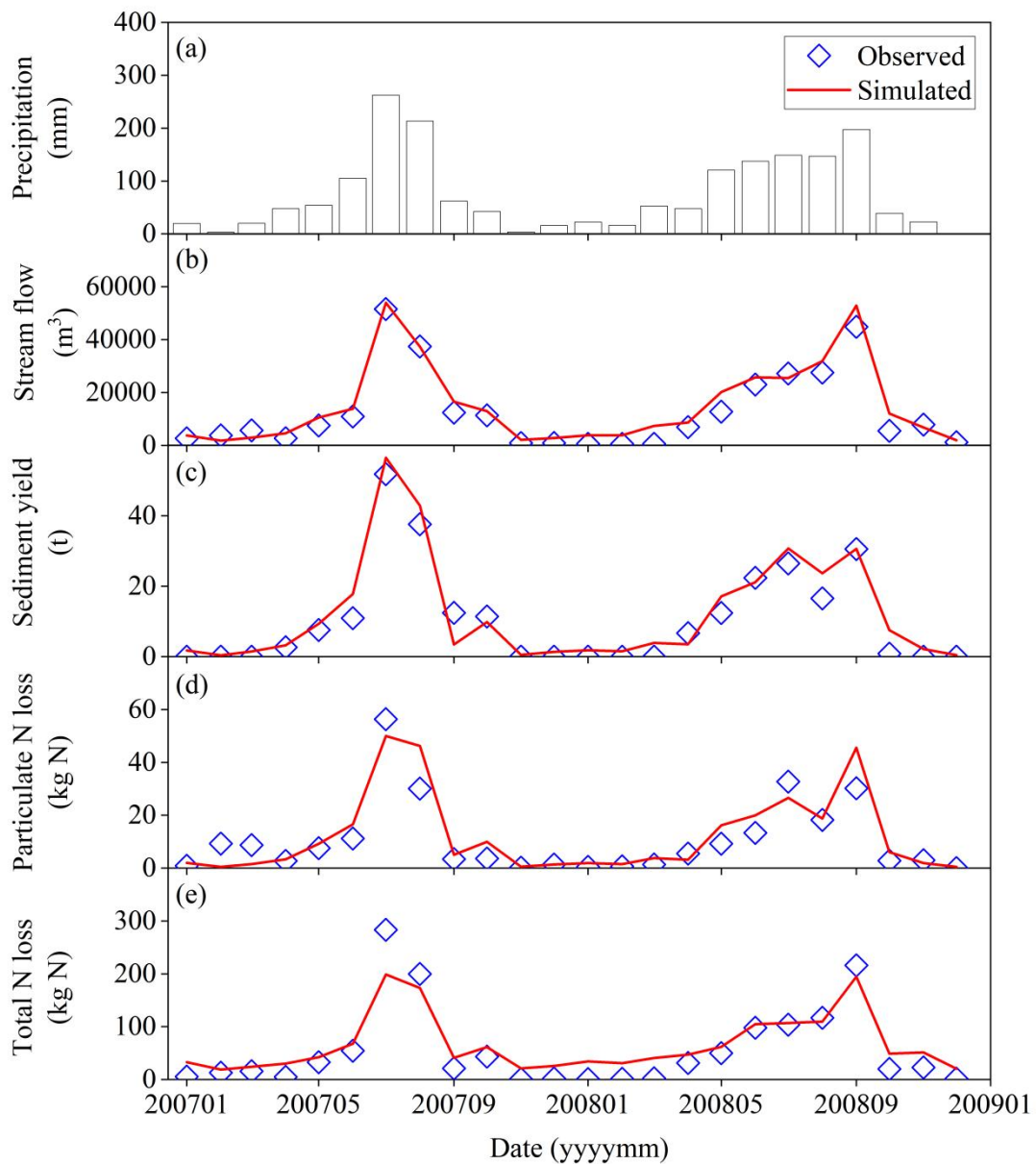
1043 dissolved and particulate P. Total N refers to the total amount of NH_4^+ , NO_3^- , dissolved organic

1044 N and particulate N. The vertical bars indicate the standard error of three spatial replicates. The

1045 observed data cited from Deng et al. (2011), Zhang et al. (2018), Li et al. (2022) and Hu (2020)

1046 were provided by Bo Zhu.

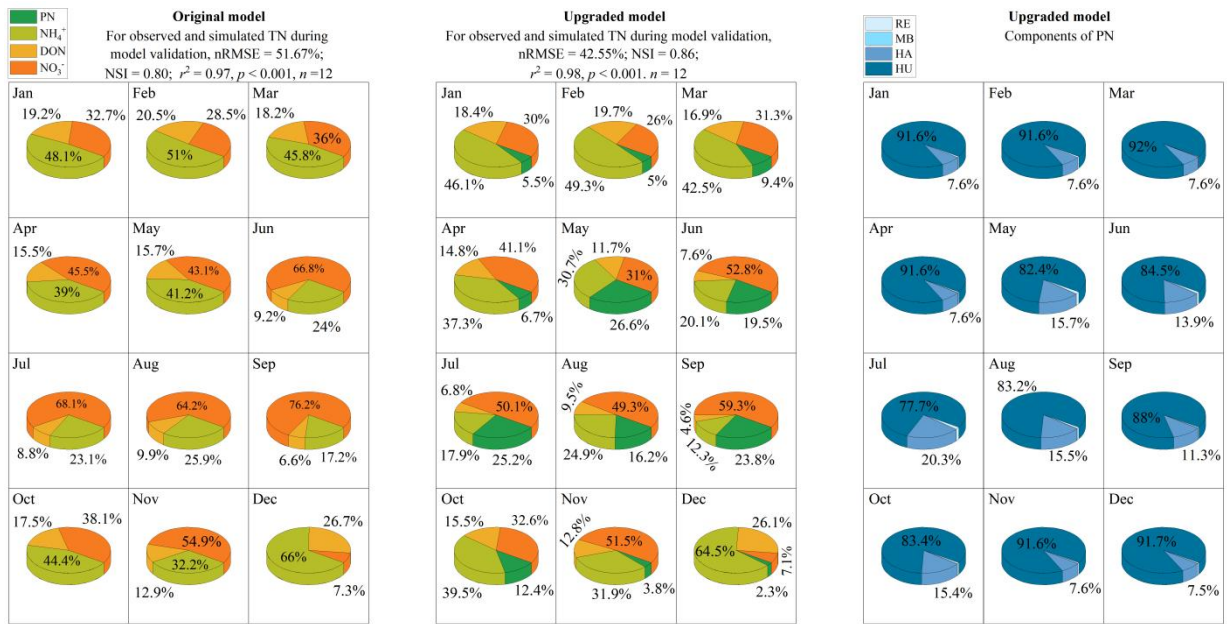
1047



1048

1049 Fig. 3 Monthly observed precipitation (a), observed and simulated stream flow (b), sediment
 1050 yield (c), particulate nitrogen (N) loss (d) and total N loss (e) at the outlet of the Jieliu
 1051 catchment from 2007 to 2008. Total N refers to the total amount of NH_4^+ , NO_3^- , dissolved
 1052 organic N and particulate N. The observed data cited from Deng et al. (2011) and Zhang et al.
 1053 (2018) were provided by Bo Zhu.

1054



1055

1056

1057

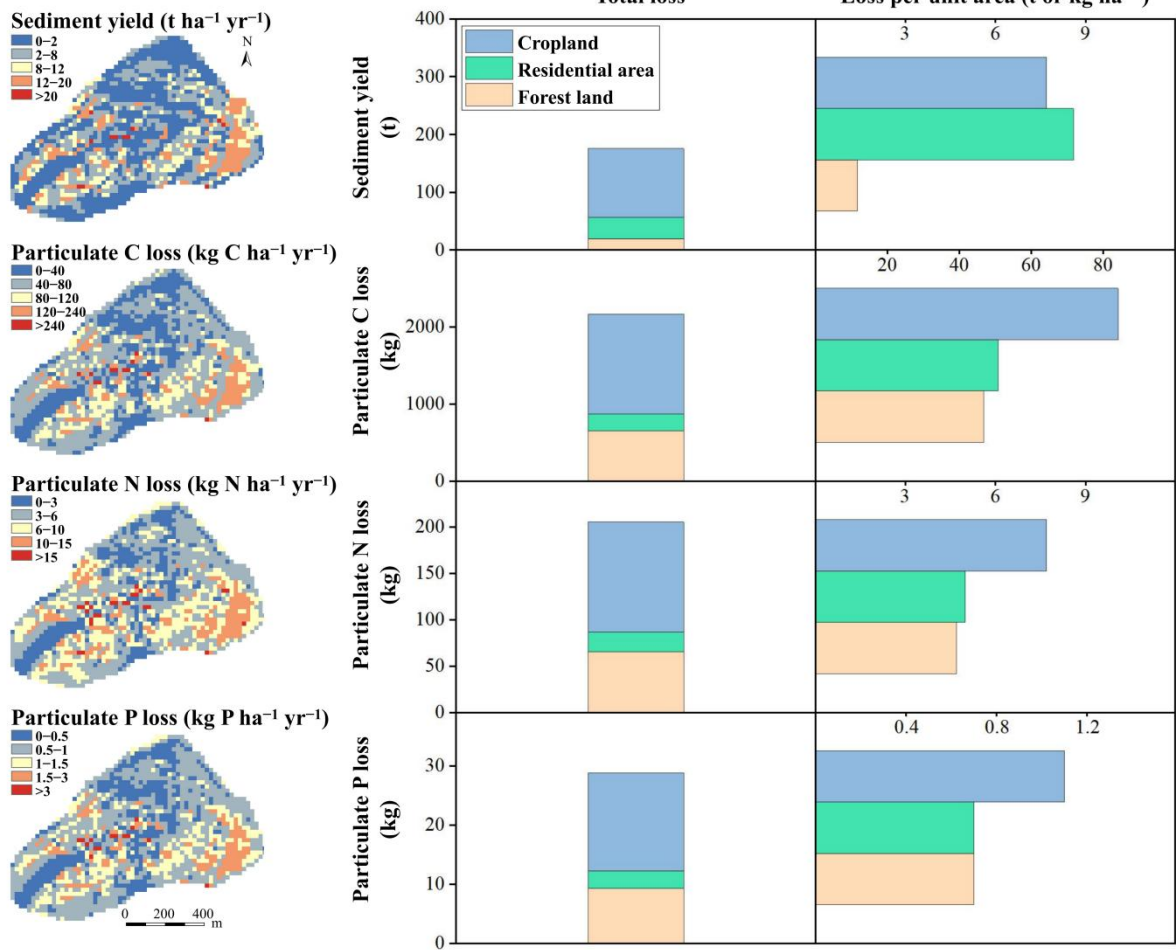
1058

1059

1060

1061

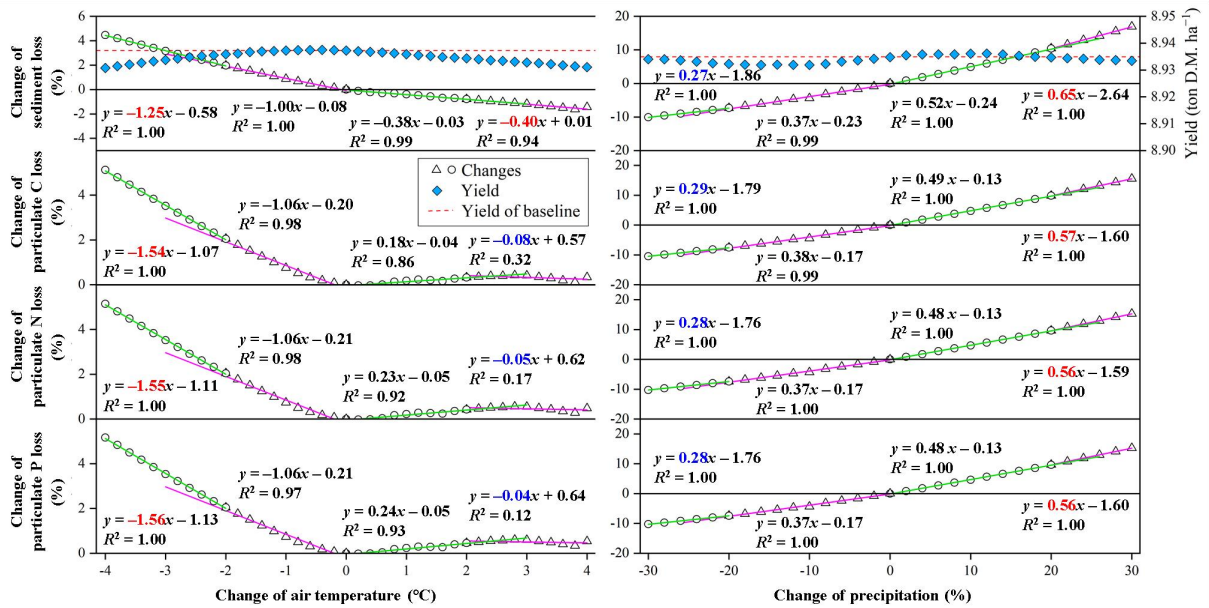
Fig. 4 Components of the simulated total nitrogen (TN) of the original CNMM-DNDC and/or components of the simulated TN and particulate N (PN) of the original and upgraded CNMM-DNDC model during the model validation. DON is the abbreviation of the dissolved organic nitrogen. The components of PN are the N from residue (RE), microbe (MB), labile or resistant humus (HA) and passive humus (HU).



1062

1063 Fig. 5 Simulated spatial distributions of sediment yield, particulate carbon (C), nitrogen (N)
 1064 and phosphorus (P) losses and the effects of different land uses (i.e., cropland, residential area
 1065 and forest land) in the validation year of 2008.

1066

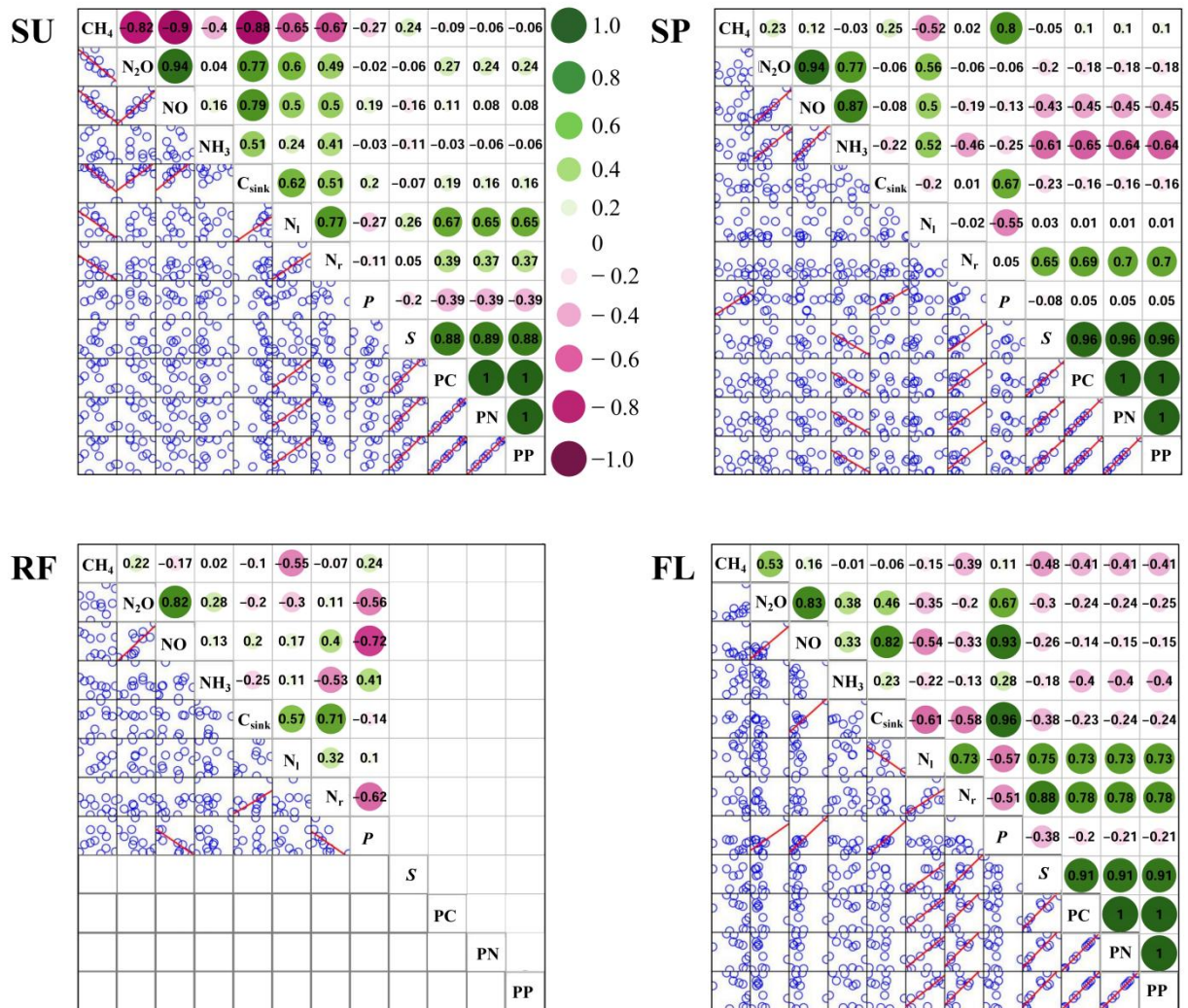


1067

1068 Fig. 6 Simulated effects of precipitation and air temperature change on sediment yield and
 1069 particulate carbon (C), nitrogen (N) and phosphorus (P) losses in the validation year of 2008.

1070 The air temperature and precipitation single-factor scenarios were divided into four sets. The
 1071 scenarios with air temperature reductions and increases 0°C~2°C and greater than 2°C were
 1072 defined as the lower and higher cooling and warming scenarios, respectively. Similarly, the
 1073 scenarios with precipitation reductions and increases 0%~20% and greater than 20% were
 1074 defined as the lower and higher rain-reduced and rain-enhanced scenarios, respectively. The
 1075 numbers in blue and red in front of the letter x represent that the higher warming or cooling
 1076 scenarios (or the higher rain-enhanced or rain-reduced scenarios) result in more and lower
 1077 effects on sediment yield and particulate C, N and P losses than the lower ones, respectively.

1078 [The green and violet lines are referred to the linear regressions between the changes of the](#)
 1079 [climate variables \(i.e., air temperature and precipitation\) and the changes of the variables](#)
 1080 [associated to soil erosion. The lines are color-coded to distinguish the results of the different](#)
 1081 [scenarios.](#)



1082

1083 Fig. 7 Correlation analysis among the simulated sediment (S), particulate carbon (PC), nitrogen
 1084 (PN) and phosphorus (PP) losses, productivity (P), C sink density (C_{sink}), methane (CH₄),
 1085 nitrous oxide (N₂O), nitric oxide (NO) and ammonia (NH₃) emissions, losses of nitrate through
 1086 leaching (N_i) and surface runoff (N_r) for different land use types. The land use types are the
 1087 sloping uplands (SU) with the summer maize–winter wheat rotation–(SU), seasonally
 1088 waterlogged paddy (SP) with the paddy rice–winter wheat rotation or paddy rice–rape rotation–
 1089 (SP), the winter-flooding paddy with the paddy rice-flooding fallow regime (RF) and the forest
 1090 land (FL). No losses of S, PC, PN, and PP in the RF crop system because of the year-round
 1091 flooding regime. The figures in the circles stand for the correlation coefficients. The

1092 ~~correlations with the level of $p < 0.05$ are considered as significant and the linear regression~~
1093 ~~lines are exhibited.~~ The scatter plots of the bottom left are relating to the correlation coefficients
1094 and the linear regression curves (i.e., the red line) are provided when the correlations with the
1095 level of $p < 0.05$ are considered as significant.